Bioorganic & Medicinal Chemistry 18 (2010) 755–768

Contents lists available at ScienceDirect

Bioorganic & Medicinal Chemistry

journal homepage: www.elsevier.com/locate/bmc

Design and preliminary structure–activity relationship of redox-silent semisynthetic tocotrienol analogues as inhibitors for breast cancer proliferation and invasion

Ahmed Y. Elnagar, Vikram B. Wali, Paul W. Sylvester, Khalid A. El Sayed *

Department of Basic Pharmaceutical Sciences, College of Pharmacy, University of Louisiana at Monroe, Monroe, LA 71201, United States

ARTICLE INFO

Article history:
Received 2 October 2009
Revised 22 November 2009
Accepted 24 November 2009
Available online 27 November 2009

Keywords:
Anti-invasive
Antiproliferative
Breast cancer
Carbamoylation
CoMFA
CoMSIA
3D QSAR
Etherification
Redox-silent
Tocotrienols
Vitamin E

ABSTRACT

Vitamin E (VE) is a generic term that represents a family of compounds composed of various tocopherol and tocotrienol isoforms. Tocotrienols display potent anti-angiogenic and antiproliferative activities. Redox-silent tocotrienol analogues also display potent anticancer activity. The ultimate objective of this study was to develop semisynthetically C-6-modified redox-silent tocotrienol analogues with enhanced antiproliferative and anti-invasive activities as compared to their parent compound. Examples of these are carbamate and ether analogues of α-, γ-, and δ-tocotrienols (**1**–**3**). Various aliphatic, olefinic, and aromatic substituents were used. Steric limitation, electrostatic, hydrogen bond donor (HBD) and hydrogen bond acceptor (HBA) properties were varied at this position and the biological activities of these derivatives were tested. Three-dimensional quantitative structure–activity relationship (3D QSAR) studies were performed using Comparative Molecular Field (CoMFA) and Comparative Molecular Similarity Indices Analyses (CoMSIA) to better understand the structural basis for biological activity and guide the future design of more potent VE analogues.

1. Introduction

Vitamin E (VE) is a generic term used for describing a family of eight different naturally occurring phenolic compounds.[1] The VE family members are further subdivided into two subgroups, tocopherols and tocotrienols.[2] Tocopherols contain a saturated phytyl side chain at C-2 while tocotrienols have an unsaturated side chain, with all *E* $\Delta^{3',7',11'}$ system. The four members of each family differ by the number and placement of methyl groups on the chromanol ring, resulting in α-, γ-, δ-tocopherols and tocotrienols.[3,4] However, individual tocopherol and tocotrienol isoforms display a wide-range of antioxidant potencies.[4] This activity shows a poor correlation to the biopotency of many antioxidant-independent actions of these compounds.[4] Evidence suggests that the level of phytyl chain saturation and/or chroman ring methylation is critical in determining the differential biopotencies demonstrated by individual VE isoforms.[1–4] Direct comparisons between the two VE subclasses showed that tocotrienols are significantly more potent than tocopherols in most biological actions, and display a consistent relationship in most instances corresponding to δ-tocotrienol ⩾ γ-tocotrienol > α-tocotrienol > δ-tocopherol > γ-, and α-tocopherol.[5,6]

VE appears to play an important role in reducing risk of cancer and cardiovascular diseases.[7–9] VE members have documented potent anti-angiogenic and antiproliferative activities.[7–9] α-Tocopherol exerts good bioavailability due to its selective recognition by transporter proteins, (e.g., alpha-tocopherol transfer (α-TT) and alpha-tocopherol-associated proteins).[7–9] Some cancer cells can inactivate VE members by rapidly metabolizing them to the corresponding carboxyethyl-hydroxychromans. Semisynthetic modifications of VE analogues targeted the improvement of their potency or to increase water solubility via the esterification of C-6 phenolic group.[10,11] Amides derived from α- and δ-tocopheramines recently reported and demonstrated improved anticancer activity.[12,13] The redox-silent analogue of **1**, 6-*O*-carboxypropyl-α-tocotrienol, showed improved anti-carcinogenic and anti-invasive activities against lung cancer A549 cells through the suppression of hypoxia adaptation of these cells by the inhibition of hypoxia-induced activation of Src signaling.[14]

The ultimate objective of this study is to design semisynthetically C-6-modified redox-silent tocotrienol analogues with enhanced anticancer effects. The accessible C-6 phenolic group was utilized to investigate the steric limitations, electronic properties

* Corresponding author. Tel.: +1 318 342 1725; fax: +1 318 342 1737.
E-mail address: elsayed@ulm.edu (K.A. El Sayed).

0968-0896/$ - see front matter © 2009 Elsevier Ltd. All rights reserved.
doi:10.1016/j.bmc.2009.11.054

and HBD and HBA characters at this position to probe and correlate the surrounding chemical tolerance and biological activity. Various aliphatic, olefinic, and aromatic substituents were selected. This study reports several new tocotrienol carbamate and ether analogues with potent antiproliferative and anti-invasive activities along with 3D QSAR analyses.

2. Results and discussion

2.1. Semisynthesis of tocotrienol analogues

Tocotrienols **1–3** were isolated from a palm oil-derived tocotrienol rich fraction (TRF) generously provided by First Tech International Ltd (Hong Kong) using normal phase vacuum liquid chromatography (VLC, hexane–dioxane, isocratic 99:1), followed by preparative HPLC (C-18 RP, isocratic H_2O–MeOH, 5:95).[15]

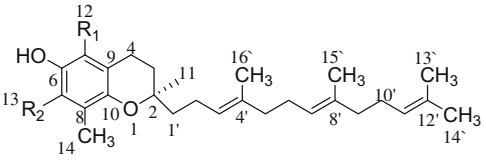

	R_1	R_2
α-tocotrienol (**1**)	CH_3	CH_3
γ-tocotrienol (**2**)	H	CH_3
δ-tocotrienol (**3**)	H	H

Reaction of diverse aliphatic, olefinic, and aromatic isocyanates with tocotrienols **1–3** afforded their corresponding C-6-carbamates **4–22**. The carbamate functionality offered alternative HBD group in these compounds, replacing the C-6 phenol moiety, in addition to the HBA carbonyl group. The HREIMS[a] data of **4** suggested the molecular formula $C_{36}H_{49}NO_5S$ and possible C-6 benzenesulfonyl carbamoylation. The ^1H and ^{13}C NMR data (Tables 1 and 2) further supported this conclusion. The aromatic protons H-4″ and H-6″ at δ_H 7.54 (Table 1) were assigned based on their ^3J-HMBC correlations with the quaternary aromatic carbon C-2″ (δ_C 139.6, Table 2). Protons H-4″ and H-6″ showed COSY coupling with H-3″/H-7″ (δ_H 8.01) as well as with H-5″ (δ_H 7.65). Proton H-5″ also showed ^3J-HMBC correlation with the aromatic methine carbons C-3″/7″ (δ_C 128.6). Thus, compound **4** was determined to be (*R*)-2,5,7,8-tetramethyl-2-((3′*E*,7′*E*)-4′,8′,12′-trimethyltrideca-3′,7′,11′-trienyl)chroman-6-yl phenylsulfonylcarbamate. C-6 Carbamoylation induced the downfield shift of C-5 (+5.1 ppm) and H-5 (+0.13) in **5**, compared to its parent **2** (Tables S1 and S2).[14] Similar downfield shift was also observed in **6** for C-5/H-5 in addition to +10.8 and 0.08 ppm shift for C-7/H-7, respectively, compared to its parent compound **3** (Tables S1 and S2).[16]

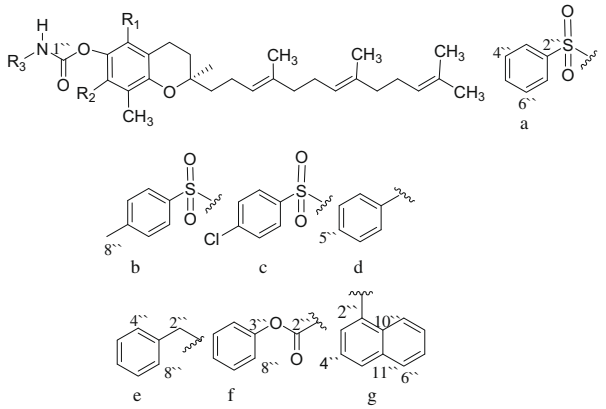

Compound	R_1	R_2	R_3
4	CH_3	CH_3	a
5	H	CH_3	a
6	H	H	a
7	CH_3	CH_3	b
8	H	CH_3	b
9	H	H	b
10	CH_3	CH_3	c
11	H	CH_3	c
12	H	H	c
13	CH_3	CH_3	d
14	H	CH_3	d
15	H	H	d
16	CH_3	CH_3	e
17	H	CH_3	e
18	H	H	e
19	CH_3	CH_3	f
20	H	CH_3	f
21	H	H	f
22	H	H	g

The HRESIMS suggested the molecular formula $C_{37}H_{51}NO_5S$. ^1H and ^{13}C NMR data of **7** indicated the presence of 6-*O*-methyl tosylcarbamate (Tables S1 and S2). The benzylic methyl group at H_3-8″ (δ_H 2.44) showed a ^2J-HMBC correlation with the quaternary aromatic carbon C-5″ (δ_C 135.6) and ^3J-HMBC correlations with the methine carbons C-4″and C-6″ (δ_C 128.6 and 129.1, respectively). Thus, compound **7** was determined to be (*R*)-2,5,7,8-tetramethyl-2-(3′*E*,7′*E*)-4′,8′,12′-trimethyltrideca-3′,7′,11′-trienyl) chroman-6-yl tosylcarbamate. Similarly, analysis of the ^1H and ^{13}C NMR data of compounds **8** and **9** (Tables 1 and 2) confirmed their identity as the chroman-6-yl tosylcarbamates of **2** and **3**, respectively.

Reaction of **1** with 4-chlorophenylsulfonylisocyante afforded compound **10**. The HREIMS data of **10** suggested the molecular formula $C_{36}H_{48}ClNO_5S$ with the *M* and *M* + 2, 3:1, isotopic cluster characteristic pattern for a monochlorinated compound. The ^1H and ^{13}C NMR (Tables 1 and 2) data showed that the 4-chlorophenylsulfonylcarbamoyl moiety has been introduced at C-6. This was based on the downfield shift of carbons C-5, C-7, and C-8 and the presence of the new carbamoyl carbonyl C-1″at δ 150.2. Therefore, compound **10** was proved to be (*R*)-2,5,7,8-tetramethyl-2-((3′*E*,7′*E*)-4′,8′,12′-trimethyltrideca-3′,7′,11′-trienyl)chroman-6-yl-4″-chlorophenylsulfonylcarbamate. Similarly, the NMR data of **11** and **12** (Tables S3 and S4) confirmed their identity as the C-6-4″-chlorophenylsulfonylcarbamate analogues of **2** and **3**, respectively.

The HRMS, ^1H, and ^{13}C NMR data of **13** (Tables S3 and S4) suggested the molecular formula $C_{36}H_{49}NO_3$ and possible C-6 phenyl carbamoylation of **1**. The aromatic protons H-4″and H-6″at δ_H 7.32 were assigned based on their ^3J-HMBC correlation with the quaternary aromatic carbon C-2″ (δ_C 145.2, Table S4). Protons H-4″/H-6″ showed COSY coupling with protons H-3″/H-7″ (δ_H 7.47) as well as with H-5″ (δ_H 7.08). Protons H-3″/H-7″ showed a ^3J-HMBC correlation with the aromatic methine carbon C-5″. Thus, compound **13** was determined to be (*R*)-2,5,7,8-tetramethyl-2-((3′*E*,7′*E*)-4′,8′,12′-trimethyltrideca-3′,7′,11′-trienyl)chroman-6-yl phenylcarbamate. Similarly, compounds **14** (Tables S3 and S4) and **15** (Tables S5 and S6) were found to be the C-6 phenylcarbamate analogues of **2** and **3**, respectively.

The HRESIMS data of **16** suggested the molecular formula $C_{37}H_{51}NO_3$. The ^1H and ^{13}C NMR data of **16** (Tables 1 and 2) suggested C-6 benzyl carbamate of **1**. The benzylic methylene protons H-2″ (δ_H 4.46) showed ^3J-HMBC correlations with H-4″/C-8″ (δ_C 127.6) C-8″ (δ_C 45.4) and the carbamate carbonyl C-1″ (δ_C 155.6). Thus, compound **16** was determined to be (*R*)-2,5,7,8-tetramethyl-2-((3′*E*,7′*E*)-4′,8′,12′-trimethyltrideca-3′,7′,11′-trienyl)chroman-6-yl benzylcarbamate. Similarly, compounds **17** and **18** (Tables S5 and S6) have been proven to be (*R*)-2,7,8-trimethyl-2-((3′*E*,7′*E*)-

Table 1
^{1}H NMR data of compounds **4**, **8**–**10**, and **16**[a]

Position	δ_H				
	4	**8**	**9**	**10**	**16**
3	1.77, m	1.75, m	1.74, m	1.73, m	1.77, m
4	2.52, m	2.63, m	2.67, m	2.53, dd (6.6, 6.6)	2.59, dd (6.6, 6.6)
5	—	6.51, s	6.58, d (6.6)	—	—
7	—	—	6.58, d (6.6)	—	—
11	1.21, s	1.23, s	1.21, s	1.95, m	1.25, s
12	1.76, s	—	—	1.22, s	2,03, s
13	1.76, s	1.84, s	—	1,79, s	2.07, s
14	2.02, s	2.04, s	2.08, s	1.79, s	2.10, s
1′	2.02, m	1.95, m	1.95, m	2.08, s	1.95, m
2′	2.05, m	2.12, m	2.00, m	2.13, m	2.13, m
3′	5.10, t (6.9)	5.11, m	5.11, m	5.10, m	5.10, m
5′	1.94, m	1.95, m	1.95, m	1.96, m	1.95, m
6′	2.00, m	2.12, m	2.07, m	2.11, m	2.11, m
7′	5.10, t (6.9)	5.11, m	5.11, m	5.10, m	5.10, m
9′	2.02, m	1.95, m	1.95, m	1.95, m	1.95, m
10′	2.07, m	2.12, m	2.07, m	2.11, m	2.11, m
11′	5.10, t (6.9)	5.11, m	5.11, m	5.10, m	5.10, m
13′	1.67, s	1.63, s	1.57, s	1.58, s	1.59, s
14′	1.58, s	1.69, s	1.66, s	1.66, s	1.67, s
15′	1.58, s	1.59, s	1.57, s	1.58, s	1.59, s
16′	1.58, s	1.59, s	1.57, s	1.58, s	1.59, s
2″	—	—	—	—	4.46, d (6.2)
3″	8.01, d (7.7)	7.94, d (8.4)	7.91, d (8.4)	7.94, d (8.1)	—
4″	7.54, dd (7.7, 7.7)	7.32, d (8.1)	7.33, d (8.4)	7.34, d (8.1)	7.30, d (6.9)
5″	7.65, dd (7.5, 7.5)	—	—	—	7.34, dd (5.8, 5.8)
6″	7.54, dd (7.7, 7.7)	7.32, d (8.1)	7.33, d(8.4)	7.33, d (8.1)	7.32, dd (5.8, 5.8)
7″	8.01, d (7.7)	7.94, d (8. 4)	7.94, d (8.4)	7.93, d (8.1)	7.34, dd (5.8, 5.8)
8″	—	2.44, s	2.44, s	—	7.30, d (6.9)

[a] In $CDCl_3$, 400 MHz. Coupling constants (*J*) are in hertz.

4′,8′,12′-trimethyltrideca-3′,7′,11′-trienyl)chroman-6-yl benzylcarbamate and (*R*)-2,8-dimethyl-2-((3′*E*,7′*E*) 4′,8′,12′-trimethyltrideca-3′,7′,11′-trienyl)chroman-6-yl benzylcarbamate, respectively.

The HREIMS data of **19** suggested the molecular formula $C_{37}H_{49}NO_5$ and possible C-6 phenylformate carbamoylation. The ^{1}H and ^{13}C NMR data (Tables S5 and S6) further supported this conclusion. The aromatic protons H-5″/H-7″ at δ_H 7.40 (Table S5) showed a ^3J-HMBC correlation with the quaternary oxygenated aromatic carbon C-3″ (δ_C 149.8, Table S6). Protons H-5″/H-7″ showed COSY couplings with H-4″/H-8″ (δ_H 7.21) as well as with H-6″ (δ_H 7.26). Thus, compound **19** was determined to be (*R*)-phenyl 2,5,7,8-tetramethyl-2-((3′*E*,7′*E*)-4′,8′,12′-trimethyltrideca-3′,7′,11′-trienyl)-chroman-6-yl iminodicarbonate. Similarly, compounds **20** and **21** (Tables S7 and S8) were shown to be (*R*)-2,7,8-trimethyl-2-((3′*E*,7′*E*)-4′,8′,12′-trimethyltrideca-3′,7′,11′-trienyl)chroman-6-yl iminodicarbonate and (*R*)-2, 8-dimethyl-2-((3′*E*,7′*E*)-4′,8′,12′-trimethyltrideca-3′,7′,11′-trienyl)-chroman-6-yl iminodicarbonate, respectively.

The HREIMS data of **22** suggested the molecular formula $C_{38}H_{47}NO_3$ and possible C-6 naphthyl carbamoylation. The ^{1}H and ^{13}C NMR data (Tables S7 and S8) further supported this conclusion. The aromatic protons H-4″ (δ_H 7.51) and H-9″ (δ_H 7.93) were assigned based on their ^3J-HMBC correlations with the quaternary aromatic carbons C-2″ and C-11″ (δ_C 135.0 and 134.0, respectively, Table S8). Proton H-9″ was COSY-coupled to H-8″ (δ_H 7.51) which showed a ^3J-HMBC correlation with C-6″ (δ_C 128.9). Furthermore, H-4″ showed COSY coupling with H-3″ and H-5″ which showed ^3J-HMBC correlations with C-10″ (δ_C 132.3). Thus, compound **22** was determined to be (*R*)-2,8-dimethyl-2-((3′*E*,7′*E*)-4′,8′,12′-trimethyltrideca-3′,7′,11′-trienyl) chroman-6-yl naphthalen-1″-yl carbamate.

Reaction of **1**–**3** with alkyl or aryl halides in THF in presence of NaH afforded the corresponding ethers **23**–**32**. The HREIMS, ^{1}H, and ^{13}C NMR data of **24** (Tables S7 and S8) suggested the molecular formula $C_{34}H_{52}O_2$ and possible C-6 etherification of **2** with a 4-methylpent-3-enyl moiety. The methylene protons H_2-1″ (δ_H 3.87) showed COSY coupling with H-2″ (δ_H 2.44). Proton H-1″ showed a ^3J-HMBC correlation with C-3″ (δ_C 110.1). Proton H-3″ (δ_H 5.22) showed ^3J-HMBC correlations with C-5″ and C-6″ (δ_C 25.7 and δ_C 17.8, respectively) and ^2J-HMBC correlation with the quaternary carbon C-4″ (δ_C 134.3). Thus, compound **24** was determined to be (*R*)-2,7,8-trimethyl-6-(4″-methylpent-3″-enyloxy)-2-((3′*E*,7′*E*)-4′,8′,12′-trimethyltrideca-3′,7′,11′-trienyl) chroman.

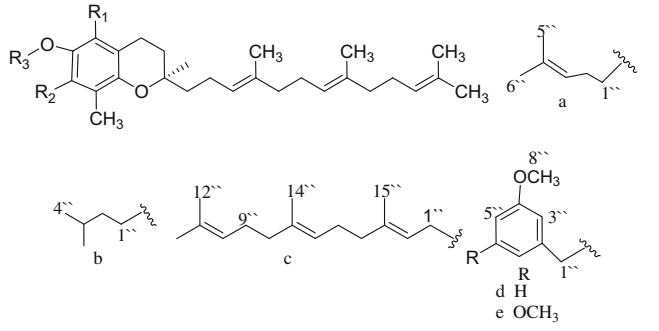

Compound	R_1	R_2	R_3
23	H	CH_3	CH_3
24	H	CH_3	a
25	H	CH_3	b
26	CH_3	CH_3	c
27	H	CH_3	c
28	H	H	c
29	CH_3	CH_3	d
30	H	CH_3	d
31	CH_3	CH_3	e
32	H	CH_3	e

The HREIMS, ^{1}H, and ^{13}C NMR data of **25** (Tables S7 and S8) suggested the molecular formula $C_{33}H_{52}O_2$ and possible C-6 isopentyl

ether analogue of **2**. The methylene protons H_2-1″ (δ_H 3.87) showed a ^3J-HMBC correlation with C-3″ (δ_C 25.2). The methyl doublets H_3-4″ and H_3-5″ (δ_H 0.95) showed ^2J-HMBC correlations with C-3″ and a ^3J-HMBC correlation with C-2″ (δ_C 22.7). Thus, compound **25** was determined to be (*R*)-6-(isopentyloxy)-2,7,8-trimethyl-2-((3′*E*,7′*E*)-4′,8′,12′-trimethyltrideca-3′,7′,11′-trienyl)chroman.

The HREIMS data of **26** suggested the molecular formula $C_{44}H_{68}O_2$. The ^{1}H and ^{13}C NMR data of **26** (Tables S9 and S10) suggested C-6 farnesyl ether of **1**. The methylene protons doublet H_2-1″ (δ_H 4.18) showed a ^3J-HMBC correlation with the quaternary oxygenated carbon C-6 (δ_C 148.0). Protons H_2-1″ showed COSY coupling with H-2″ (δ_H 5.58). Proton H-1″ also showed a ^3J-HMBC correlation with C-3″ (δ_C 140.6). The methyl protons singlet H_3-15″ (δ_H 1.60) showed ^3J-HMBC correlations with C-2″ and C-4″ (δ_C 124.2 and 39.8, respectively) and a ^2J-HMBC correlation with C-3″, connecting the isoprenyl segment C-1″-C-4″/C-15″. Similarly, the other two isoprenyl segments C-5″-C-8″/C-14″ and C-9″-C-13″ were confirmed. Thus, compound **26** was determined to be (*R*)-2,5,7,8-tetramethyl-6-(2″*E*,6″*E*)-3″,7″,11″-trimethyldodeca-2″,6″,10″-trienyloxy)-2-((3′*E*,7′*E*)-4′,8′,12′-trimethyltrideca-3′,7′,11′-trienyl)chroman. Similarly, compounds **27** and **28** (Tables S9 and S10) have been proven to be (*R*)-2,7,8-trimethyl-6-(2″*E*,6″*E*)-3″,7″,11″-trimethyldodeca-2″,6″,10′-trienyloxy)-2-((3′*E*,7′*E*)-4′,8′,12′-trimethyltrideca-3′,7′,11′-trienyl)chroman and (*R*)-2,8-dimethyl-6-((2″*E*,6″*E*)-3″,7″,11″-trimethyldodeca-2″,6″,10″-trienyloxy)-2-((3′*E*,7′*E*)-4′,8′,12′-trimethyltrideca-3′,7′,11′-trienyl)chroman.

Table 2
^{13}C NMR data of compounds **4**, **8**–**10**, and **16**[a]

Position	δ_C				
	4	**8**	**9**	**10**	**16**
2	75.0, qC	76.0, qC	76.1, qC	75.1, qC	76.1, qC
3	31.0, CH_2	30.9, CH_2	30.9, CH_2	31.0, CH_2	31.2, CH_2
4	20.5, CH_2	22.2, CH_2	22.2, CH_2	22.2, CH_2	20.6, CH_2
5	117.5, qC	118.7, qC	120.8, CH	123.6, qC	117.3, CH
6	138.4, qC	140.6, qC	141.8, qC	140.0, qC	140.9, qC
7	125.3, qC	126.1, qC	118.8, CH	125.5, qC	125.5, qC
8	126.9, qC	127.1, qC	127.8, qC	127.1, qC	125.9, qC
9	123.3, qC	118.5, qC	121.0, qC	117.5, qC	123.0, qC
10	149.9,qC	149.3,qC	150.4,qC	149.2, qC	149.6, qC
11	23.8 CH_3	24.1 CH_3	24.1, CH_3	24.1, CH_3	23.9, CH_3
12	11.7, CH_3	11.7, CH_3	—	11.7, CH_3	11.9, CH_3
13	12.5, CH_3	12.5, CH_3	—	11.8, CH_3	13.2, CH_3
14	11.8, CH_3	11.8, CH_3	14.1, CH_3	12.5, CH_3	11.9, CH_3
1′	39.8, CH_2	40.0, CH_2	40.0, CH_2	39.7, CH_2	39.8, CH_2
2′	22.2, CH_2	22.2, CH_2	22.2, CH_2	20.5, CH_2	22.2, CH_2
3′	124.4, CH	124.1, CH	124.1, CH	124.4, CH	124.4, CH
4′	135.0, CH_2	135.3, CH_2	135.3, CH_2	135.5, qC	135.2, qC
5′	39.8, CH_2	39.7, CH_2	39.7, CH_2	39.7, CH_2	39.7, CH_2
6′	26.6, CH_2	26.6, CH_2	26.6, CH_2	26.6, CH_2	26.6, CH_2
7′	124.2, CH	124.2, CH	124.2, CH	124.2, CH	124.2, CH
8′	135.0, qC	135.3, qC	135.3, qC	135.3, qC	135.0, qC
9′	39.8, CH_2	39.7, CH_2	39.7, CH_2	39.7, CH_2	39.7, CH_2
10′	26.8, CH_2	26.8, CH_2	26.8, CH_2	26.8, CH_2	26.8, CH_2
11′	124.2, CH	124.2, CH	124.2, CH	124.1, CH	124.4, CH
12′	131.3, qC	131.3, qC	131.3, qC	131.2, qC	131.8, qC
13′	25.8, CH_3	25.8, CH_3	25.8, CH_3	25.7, CH_3	25.8, CH_3
14′	17.8, CH_3	17.8,CH_3	17.8, CH_3	17.9, CH_3	18.0, CH_3
15′	16.1, CH_3	16.1, CH_3	16.1, CH_3	16.0, CH_3	16.4, CH_3
16′	16.0, CH_3	16.0, CH_3	15.9, CH_3	15.9, CH_3	16.3, CH_3
1″	149.1, qC	150.0, qC	150.8, qC	150.2, qC	155.6, qC
2″	139.6, qC	145.3, qC	145.1, qC	145.2,qC	45.4, CH_2
3″	128.6,CH	128.6, CH	128.5, CH[b]	129.7, CH	139.1, qC
4″	129.1,CH	129.7, CH	129.7, CH[c]	128.6, CH	127.6, CH
5″	134.1,CH	135.0, qC	135.0, qC	135.6, qC	129.4, CH
6″	129.1,CH	129.7, CH	128.6, CH[c]	128.6, CH	136.7, qC
7″	128.6,CH	128.6, CH	129.6, CH[b]	129.7, CH	129.4, CH
8″	—	21.7 CH_3	21.7, CH_3	—	127.6, CH

[a] In $CDCl_3$, 100 MHz. Carbon multiplicities were determined by DEPT135° or APT experiments. qC = quaternary, CH = methine, CH_2 = methylene, CH_3 = methyl carbons.
[b,c] Interchangeable within the same column.

The HREIMS data of **29** suggested the molecular formula $C_{37}H_{52}O_3$. The ^{1}H and ^{13}C NMR data (Tables S11 and S12) suggested that compound **29** is a C-6 4-methoxybenzyl ether analogue of **1**. The benzylic methylene protons H_2-1″ (δ_H 4.66) showed ^3J-HMBC correlations with the quaternary carbon C-6 (δ_C 147.9) and the aromatic methine carbons C-3″ and C-7″ (δ_C 119.9 and 113.3, respectively), connecting the new 4-methoxybenzyl ether with the chroman ring of **1**. The aromatic proton singlet H-3″ (δ_H 7.03) showed ^3J-HMBC correlations with the aromatic methine carbons C-5″ (δ_C 113.1) and C-7″. The proton doublet of doublet H-6″ (δ_H 7.30) showed ^3J-HMBC correlations with the quaternary carbons C-2″ and C-4″at (δ_C 139.8 and 160.2, respectively). A double doublet proton H-6″ showed the COSY coupling with H-7″ at δ_H 7.30. The methoxy singlet H_3-8″ (δ_H 3.86) showed a ^3J-HMBC correlation with C-4″. Thus, compound **29** was determined to be (*R*)-6-(4″-methoxybenzyloxy)-2,5,7,8-tetramethyl-2-((3′*E*,7′*E*)-4′,8′,12′-trimethyltrideca-3′,7′,11′-trienyl)chroman. Compound **30** was assigned in a similar manner based on the ^{1}H and ^{13}C NMR data (Tables S11 and S12) and was determined to be (*R*)-6-(4″-methoxybenzyloxy)-2,7,8-trimethyl-2-((3′*E*,7′*E*)-4′,8′,12′-trimethyltrideca-3′,7′,11′-trienyl)chroman.

The HREIMS data of **31** suggested the molecular formula $C_{38}H_{54}O_4$. The ^{1}H and ^{13}C NMR data (Tables S11 and S12) was closely similar to those of **29** with C-6 (4″, 6″-dimethoxybenzyloxy moiety. The methoxy proton singlets H_3-8″ and H_3-9″ (δ_H 3.81) showed ^3J-HMBC correlations with carbons C-4″ and C-6″ (δ_C 160.9). Thus, compound **31** was determined to be (*R*)-6-(4″,6″-dimethoxybenzyloxy)-2,5,7,8-tetramethyl-2-((3′*E*,7′*E*)-4′,8′,12′-trimethyltrideca-3′,7′,11′-trienyl)chroman. Similarly, compound **32** was assigned based on the ^{1}H and ^{13}C NMR data (Table S13) and was determined to be (*R*)-6-(4″,6″-dimethoxybenzyloxy)-2,7,8-trimethyl-2-((3′*E*,7′*E*)-4′,8′,12′-trimethyltrideca-3′,7′,11′-trienyl) chroman.

2.2. Biological activity

Tocotrienols **1**–**3** are significantly more potent than tocopherols in suppressing tumor cell growth and viability. The anticancer effects of tocotrienols are observed using treatments doses that have little or no effect on normal cell function or viability.[4,7] Recent findings also suggest that the antiproliferative γ-tocotrienol may occur upstream of the PI3K/PDK-1/AKT mitogenic signaling pathway at the level of the EGF-receptor.[4,14] The antiproliferative effects of γ-tocotrienol on neoplastic +SA mammary epithelial cells are mediated through the reduction in ErbB3 tyrosine phosphorylation and subsequent activation of the PI3K/PDK-1/AKT mitogenic signaling pathway.[4,14] Treatment with a growth inhibitory, but not cytotoxic dose of γ-tocotrienol, results in approximately a 50% reduction in EGF-dependent +SA cell growth, and these effects are associated with a corresponding decrease in phospho-AKT (active) levels in these cells, and this lead finally to apoptosis and cell death.[4,13,17]

The antiproliferative and anti-invasive activities of **1**–**32** were evaluated using MTT and cell invasion assay kits, respectively. The antiproliferative activity has been evaluated against the highly malignant +SA mouse mammary epithelial cells and the human breast cancer MCF-7 and MDA-MB-231 cell lines. The later cell line was also used for the assessment of the anti-invasive activity. With its documented antiproliferative activity, **2** was used as a positive control in all biological assays.[13] MTT-assay detects the living, but not dead cells, in quantitative colorimetric fashion utilizing cellular ability to reduce the MTT to insoluble purple formazan dye.[17] Therefore, this method is routinely used to assess the cytotoxicity and proliferation inhibitory activities.

While many of the prepared semisynthetic tocotrienols retained the activity, some of them were more active than the starting natural products. Compound **8** was the most active against +SA mouse mammary epithelial cells with an IC_{50} 2 μM, which repre-

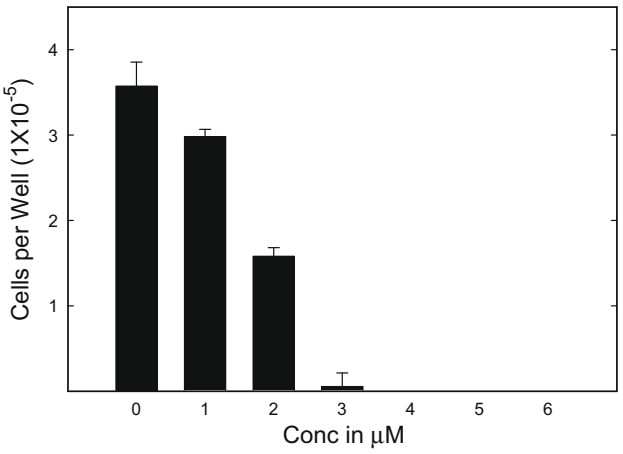

Figure 1. Antiproliferative activity of the most active analogue **8** against the highly malignant mouse +SA mammary epithelial cells.

sents nearly twofold the activity of its parent γ-tocotrienol (**2**) (Fig. 1). Compounds **4**, **6**, **8**, **10**, and **21** showed improved activities against the ER-positive human breast cancer cells MCF7 compared to the starting natural products **1**–**3** (Fig. 2). Tocotrienols **4**, **8**, and **10** with IC_{50} 5–10 μM were the most active (Table 3). Compounds **4** and **10** are eightfold more active than their parent **1**. Compound **8** was nearly threefold as active as its parent **2** (Fig. 2). Compounds **9**, **13**, **16** and **17** showed improved activities against the ER-negative human breast cancer cells MDA-MB-231 (Fig. 3). The most active compound was **9** with an IC_{50} range of 5–10 μM (Table 3).

A number of studies discussing the ability of tocotrienols to inhibit tumor cells invasion and migration were reported.[18] The anti-migratory activity was usually correlated with the anti-angiogenic activity, especially for δ-tocotrienol.[19] Recently, the anti-invasive and anti-migratory activities of **2** against the human gastric adenocarcinoma, melanoma, and prostate cancer cells were reported.[20]

The anti-invasive activities of tocotrienols **1**–**32** were measured using a 96 well basement membrane extract (BME) cell invasion assay kit against the highly metastatic MDA-MB-231 cells.[21,22] This assay employs a simplified Boyden Chamber design with a polyethylene terephthalate membrane (8 μm). Detection of cell invasion is quantified using calcein–acetomethylester (calcein–AM).[21,22] Cells internalize calcein–AM and intracellular esterases cleave the acetomethylester moiety to generate free calcein. Free calcein fluoresces brightly, and this fluorescence may be used to quantify the number of cells that have invaded across BME.[21,22] The most active analogue **16**, α-tocotrienol-6-benzylcarbamate, allowed only 8% of MDA-MB-231 cells to migrate (Fig. 4), which suggests that introduction of a bulky aromatic moiety at an optimum distance from the 6-oxygen atom along with carbamate moiety (benzyl carbamate) can enhance the anti-invasive activity of **1**. This

Table 3
Antiproliferative activity of tocotrienols **1**–**21** against the human breast cancer cell lines MCF-7 and MDA-MB-231

Compound	IC_{50} μM MDA-MB-231	IC_{50} μM MCF7
1	>10	>20
2	>10	11.4 ± 1.53
3	>10	15.5 ± 0.40
4	>10	4.5 ± 1.02
5	>10	>20
6	>10	6.1 ± 1.40
7	>10	6.1 ± 1.67
8	>10	2.4 ± 0.35
9	6.6 ± 1.70	>20
10	>10	5.1 ± 0.45
11	>10	>20
12	>10	>20
13	>10	>20
14	>10	>20
15	>10	>20
16	7.2 ± 0.56	>20
17	>10	>20
18	>10	>20
19	>10	>20
20	ND	>20
21	ND	5.6 ± 0.56
33	ND	12 ± 2
34	ND	>368
35	ND	329 ± 12

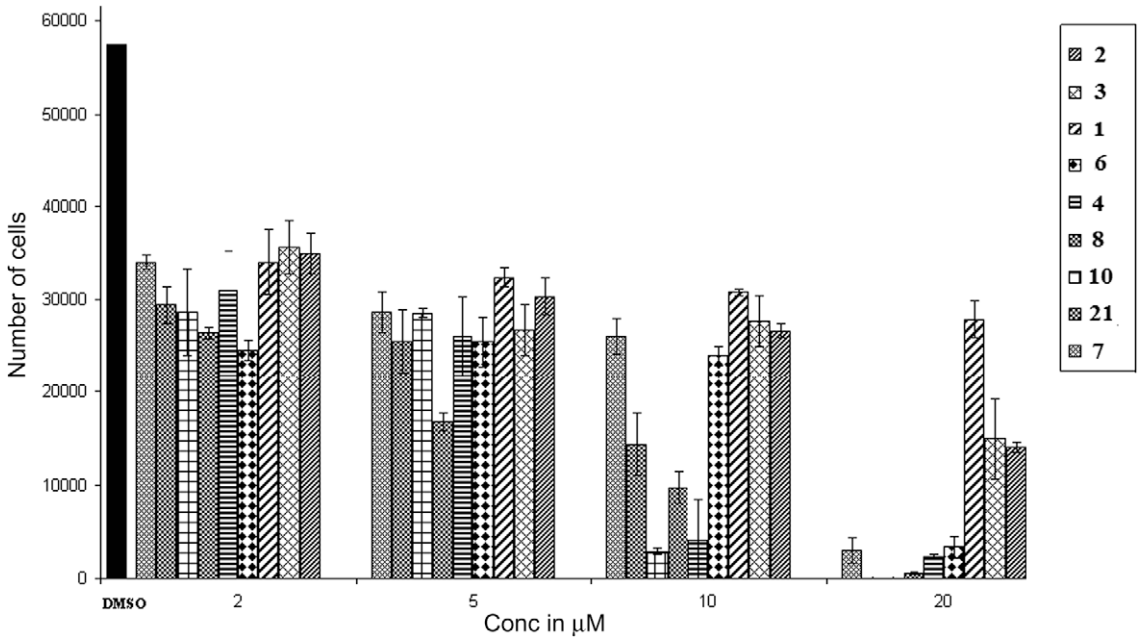

Figure 2. Antiproliferative activity of tocotrienol analogues against MCF-7 cells.

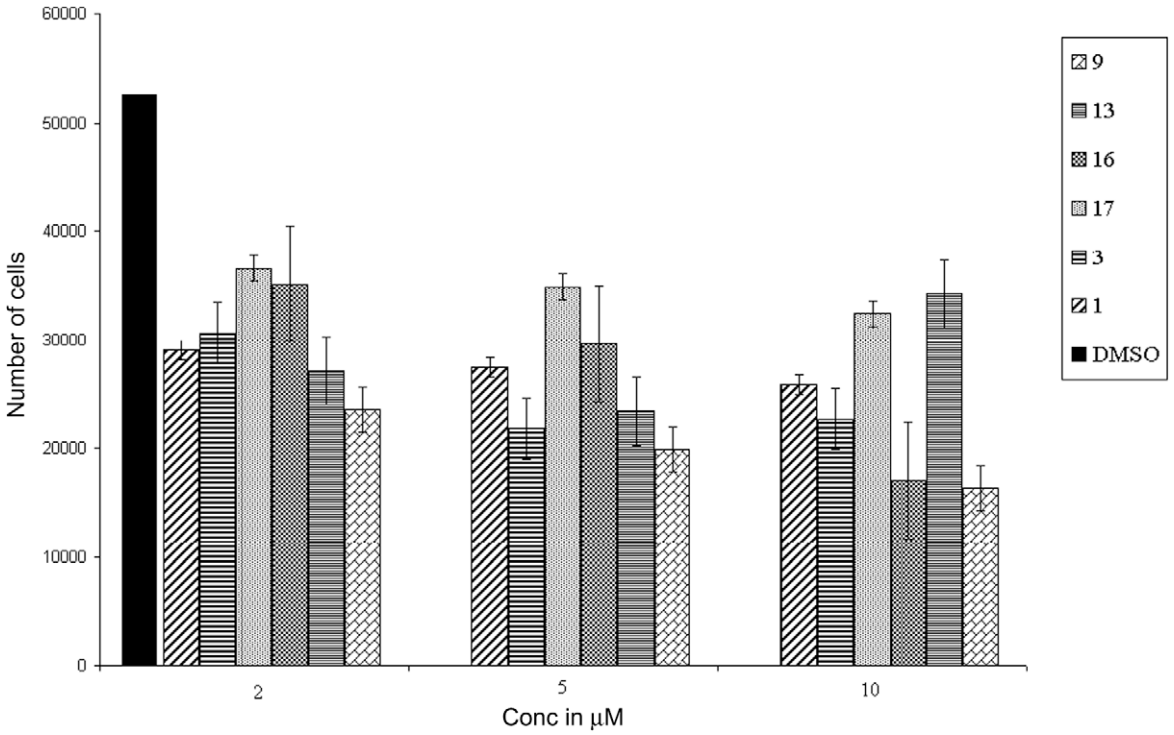

Figure 3. Antiproliferative activity of tocotrienol analogues **9**, **13**, **16**, and **17** against MDA-MB-231 cells.

was further supported by the improved activity of **17** (γ-tocotrienol-6-benzylcarbamate) and **9** (δ-tocotrienol-6-tosylcarbamate) compared to their parent compounds **2** and **3** (Fig. 4). Meanwhile, all redox-silent ethers **23**–**32** did not show any significant activity, which proves the importance of the carbamate moiety and the requirement of at least a HBD functionality at an optimized distance of C-6 oxygen for the activity.

2.3. 3D QSAR studies

Classical QSAR correlates biological activities of drugs with physicochemical properties or indicator variables which encode certain structural features.[23] In addition to lipophilicity, polarizability, and electronic properties, steric parameters are also frequently used to describe different size of substituents. In some cases, indicator variables have been attributed to differentiate racemates and active enantiomers.[23]

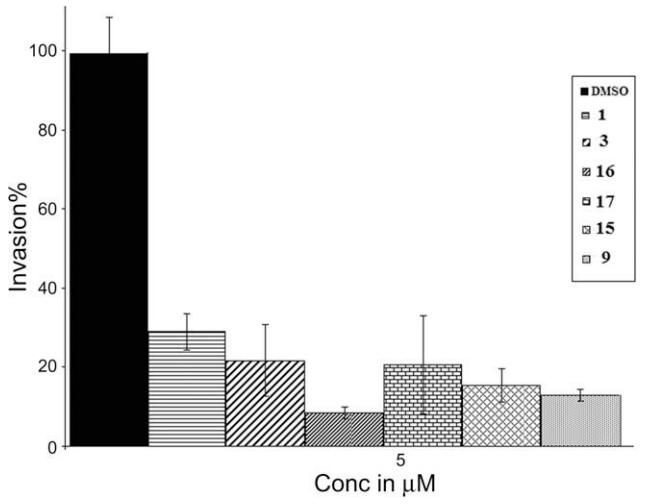

Figure 4. Anti-invasive activities of 5 μM dose of tocotrienol analogues **12**, **13**, **16**, and **23** against MDA-MB-231 cells using Cultrex™ assay kit.

Since there is no previous report for 3D QSAR model for tocotrienols, it is important to build a QSAR model to predict and optimize the properties and activities of future untested tocotrienol analogues and determine key structural requirements for enhanced activity. Accordingly, 3D QSAR models for tocotrienols were designed using the most widely used computer-based methodologies, CoMFA and CoMSIA.[23]

In order to widen the range of bioactivity, the previously published tocopherol esters **33** and **34** were considered for their known antiproliferative activities against MCF7.[24] The actual and predicted (by CoMFA and CoMSIA) pIC_{50} for the tocotrienol and tocopherol series are listed in Tables 4 and 5. Partial least square (PLS), the statistical method used in deriving the 3D QSAR models, is a variation of principal component regression in which the original variables are replaced by a small set of linear combinations.[25] The generated latent variables were used for multivariate regression, maximizing the communality of predictor and response variable blocks. Initial leave-one-out (LOO) cross-validated PLS analyses were used to determine the optimum number of components to be used in the final QSAR models.

2.3.1. CoMFA models

PLS analysis of the multifit alignment of all compounds in the training set using CoMFA-STD resulted in a CoMFA QSAR model with a good q^2 value of 0.601 (Table 6). The PLS stdev* coefficient contour maps for the CoMFA model are shown in Figures 5 and 6. Green regions indicate areas where steric bulk is predicted to enhance biological activity, whereas yellow contours indicate regions where steric bulk is predicted to be detrimental to the activity. The bulky benzene or *p*-toluenesulfonyl moieties are located in the green contour area (Fig. 5), which justifies the enhanced activity of these analogues. Blue-colored regions indicate areas where electropositive groups are predicted to enhance the biological activity while red regions are areas where electronegative groups are

Table 4
Actual, predicted, and residual of predictions of the test set by the CoMFA and CoMSIA models

Compound	Actual pIC_{50}	Predicted CoMFA pIC_{50}	CoMFA residuals	Predicted CoMSIA pIC_{50}	CoMSIA residuals
4	1.651	1.529	0.121	1.711	−0.060
2	2.051	1.934	0.117	2.001	0.050
25	2.690	2.682	0.008	2.631	0.059
32	2.690	2.752	−0.062	2.688	0.002
24	2.872	2.961	−0.089	2.994	−0.122

predicted to favor activity (Fig. 6). The most active analogue, **8**, possesses an electropositive charge around the NH-moiety near the blue contour, and an electronegative charge around the sulfone and benzene groups, near the red contour justifying improved activity. Lower energy cutoff values of 25 and 20 kcal/mol were also investigated but they all led to a decrease in the q^2 value.

2.3.2. CoMSIA models

CoMSIA is less affected by changes in molecular alignment and provides smoother and better interpretable contour maps as a result of employing Gaussian type distance dependence with the molecular similarity indices it uses. In addition to the steric and electrostatic fields, CoMSIA defines explicit hydrophobic and HBD and HBA descriptor fields, which are not available in standard CoMFA. CoMSIA also offers more fields of activity prediction. Several trials were attempted using default SYBYL CoMSIA parameters and all compounds in the training set (Table 5) with the field fit molecular alignment resulted in a PLS model with a better q^2 value of 0.651, compared to a q^2 value of 0.601 for CoMFA, and an r^2 value of 0.993 for 10 PLS components (Table 6). Hydrophobic, HBD and HBA, electrostatic, and steric descriptors were used. Only hydrophobic, steric, and electrostatic descriptors were proven to be better descriptors for tocotrienols SAR, Figures 7–9, because whenever other descriptors were used a lower q^2 value (0.305) was obtained (Table 6).

The CoMSIA-derived hydrophobic fields (Fig. 7, yellow, hydrophobic group favored; white, hydrophobic disfavored) correlate the biological activity and hydrophobicity features of tocotrienols. Hydrophobic properties around benzene ring is more favorable but not favorable around the NH or sulfone moiety in the most active compound **8**. CoMSIA also suggested the importance of hydrophobicity around the isoprenyl side chain of tocotrienols. Similar to CoMFA, green regions indicate areas where steric bulk is predicted to enhance the antiproliferative activity, whereas yellow contours indicate regions where steric bulky groups are expected to reduce the activity (Fig. 8). The green contour in case of compound **8** suggests that bulky groups like *p*-toluene and sulfone will increase the antiproliferative effect of tocotrienols. Blue and red contours indicate areas where electropositive and electronegative groups, respectively, are expected to enhance the activity (Fig. 9). This was illustrated in **8** where the sulfone moiety was located in the red area while the NH-moiety was near to the blue one.

Based on 3D QSAR results, new analogues (**36**–**40**) with enhanced activity have been designed to confirm the predictivity of the model. Compound **8**, the most active analogue, was considered as a scaffold. Antiproliferation IC_{50} values of **36**–**40** against MCF-7 cell line were calculated using the CoMSIA model (Table 7). This was based on the fact that introducing a hydrophilic group in *p*-position of benzenesulfonyl carbamate moiety will enhance the activity. Compound **36** with a 4″, 5″, and 6″-trihydroxy substitution was the most active. Compounds **39** with a 4″-carboxy and **37** with 4″ and 5″-dihydroxy substitutions were the next most potent. This clearly demonstrates the preference of hydroxyl and carboxyl groups over the amino groups since compound **40** with C-5″ amino group was the least potent.

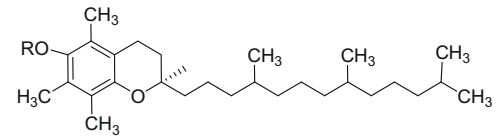

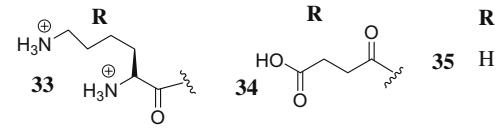

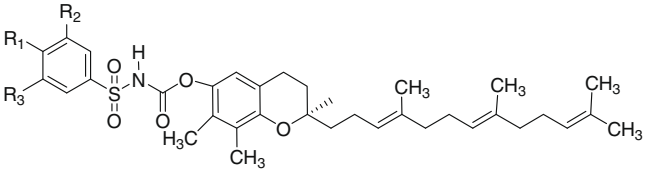

Compound	R_1	R_2	R_3
36	OH	H	H
37	OH	OH	H
36	OH	OH	OH
39	COOH	H	H
40	NH_2	H	H

3. Conclusions

Tocotrienols are potent antiproliferative and anti-invasive natural products. To probe the chemical space around the C-6 phenol group, several redox-silent carbamate and ether analogues were prepared. It has been shown that a HBD at an optimized distance of C-6 oxygen is required for the activity. 3D QSAR analyses were performed for the first time to tocotrienols and their models provide a guide for future design of more potent analogues. 3D QSAR models have good cross-validated q^2 values, suggesting a good predictive ability. The 3D contour plots derived in this study may assess the future development of tocotrienol-based antiproliferative and anti-invasive entities.

4. Material and methods

4.1. General experimental procedures

Optical rotations were measured on a Rudolph Research Analytical Autopol III polarimeter. IR spectra were recorded on a Varian 800 FT-IR spectrophotometer. The ^1H and ^{13}C NMR spectra were recorded in $CDCl_3$, using TMS as an internal standard, on a JEOL Eclipse NMR spectrometer operating at 400 MHz for ^1H and 100 MHz for ^{13}C. The HREIMS experiments were conducted at the University of Michigan on a Micromass LCT spectrometer. Analytical HPLC analyses were performed on a DIONEX® Summit II instrument on a Phenomenex Luna 250 × 4.6 mm, RP-C_{18} column using MeOH–H_2O (9.5:0.5)

Table 5
Actual, predicted, and residual of predictions of the training set by the CoMFA and CoMSIA models

Compound	Actual pIC_{50}	Predicted CoMFA pIC_{50}	CoMFA residuals	Predicted CoMSIA pIC_{50}	CoMSIA residuals
8	1.380	1.383	−0.003	1.383	−0.003
10	1.707	1.715	−0.008	1.695	0.012
21	1.748	1.725	0.023	1.725	0.023
6	1.780	1.733	0.047	1.773	0.007
7	1.786	1.794	−0.008	1.82	−0.034
33	2.081	2.081	0	2.081	0
3	2.190	2.122	0.068	2.122	0.068
19	2.690	2.73	−0.04	2.698	−0.008
13	2.690	2.711	−0.021	2.711	−0.021
22	2.690	2.692	−0.002	2.692	−0.002
11	2.690	2.719	−0.029	2.719	−0.029
17	2.690	2.673	0.017	2.673	0.017
14	2.690	2.732	−0.042	2.732	−0.042
28	2.690	2.742	−0.052	2.742	−0.052
20	2.690	2.797	−0.107	2.797	−0.107
27	2.690	2.687	0.003	2.687	0.003
26	2.690	2.695	−0.005	2.695	−0.005
29	2.690	2.693	−0.003	2.693	−0.003
30	2.690	2.74	−0.05	2.74	−0.05
31	2.690	2.648	0.042	2.648	0.042
12	2.693	2.718	−0.025	2.693	0
1	2.795	2.724	0.071	2.724	0.071
9	2.870	2.904	−0.034	2.904	−0.034
16	3.003	2.977	0.026	3	0.003
5	3.040	2.929	0.111	2.929	0.111
35	3.517	3.442	0.075	3.442	0.075
34	3.565	3.571	−0.006	3.571	−0.006

Table 6
PLS statistics of CoMFA and CoMSIA 3D QSAR (multifit alignment)

PLS statistics	CoMFA model	CoMSIA model
q^2	0.601	0.651
r^2 Conventional	0.989	0.993
Std. error	0.022	0.039
F value	272.061	251.359
P value	0.000	0.000
PLS components	7	10
Field contribution		
Steric	0.540	0.209
Electrostatic	0.460	0.458
Hydrophobic		0.333

q^2, cross-validated correlation coefficient; r^2, correlation coefficient; *F*, *F*-test value.

isocratic elution with UV detection set at 295 nm to verify the purity of each compound. A purity of >95% has been established for all compounds except **11** and **12**, where 90% purity has been established. TLC analysis was carried on precoated Si Gel 60 F_{254} 500 μm TLC plates (EMD Chemicals), using *n*-hexane–EtOAc (8:2) or $CHCl_3$–MeOH (9:1) as developing systems. For column chromatography, Si Gel 60 (Natland, 63–200 μm), *n*-hexane–EtOAc (9.5:0.5), and *n*-hexane–$CHCl_3$ (6:4) systems were used.

4.2. Chemical reactions

(A) Carbamoylation of **1**–**3**.[26] To solutions of **1–3** in toluene (2 mL), different isocyanates and 10 μL of triethylamine (Et_3N)

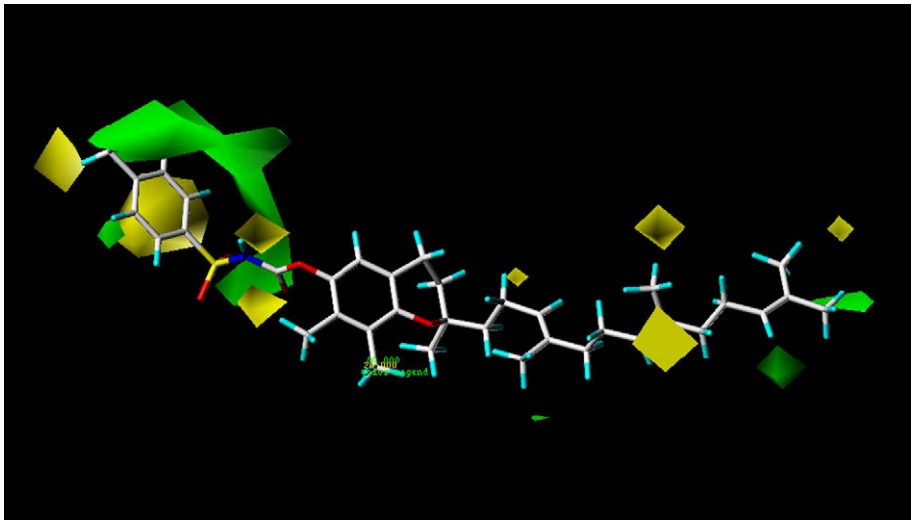

Figure 5. CoMFA steric contours plots; green contours indicate regions where bulky groups increase activity, whereas yellow contours indicate regions where bulky groups decrease activity.

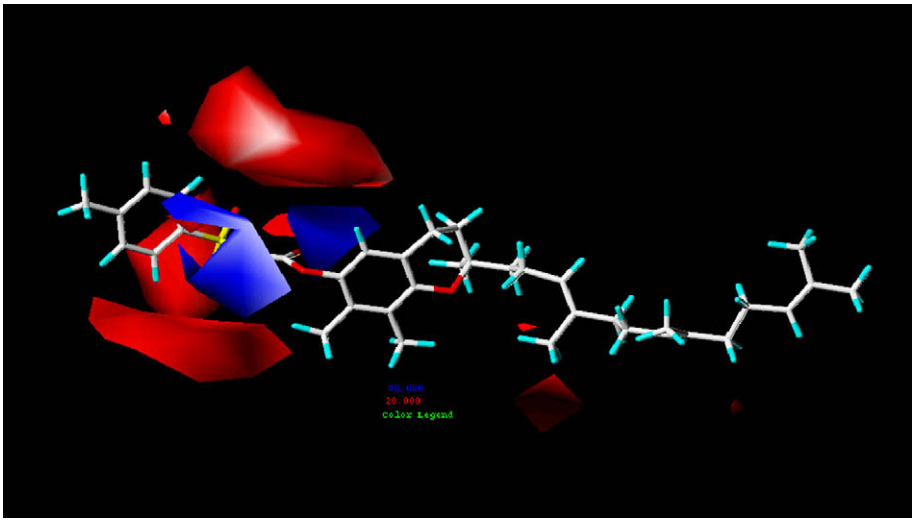

Figure 6. CoMFA stdev * coeff electrostatic contour plots; Blue contours indicate regions where positive groups increase activity, whereas red contours indicate regions where negative charge increases activity.

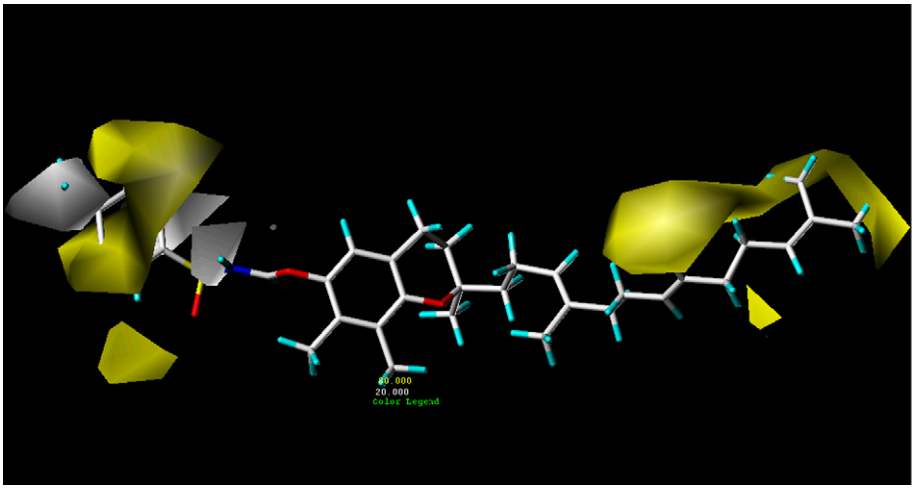

Figure 7. CoMSIA stdev * coeff hydrophobic contour plots; yellow contours indicate regions where hydrophobic (lipophilic) groups increase activity, whereas white contours indicate regions where hydrophobic (lipophilic) groups decrease activity.

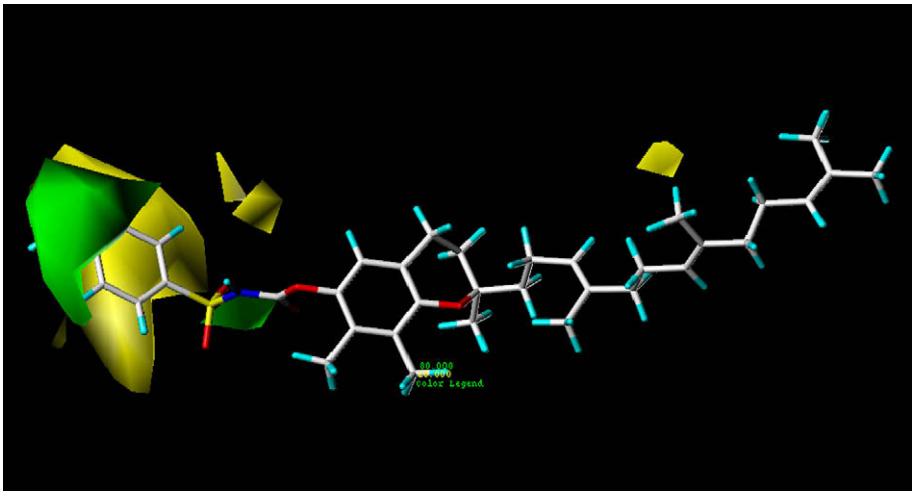

Figure 8. CoMSIA steric contours plots; green contours indicate regions where bulky groups increase activity, whereas yellow contours indicate regions where bulky groups decrease activity.

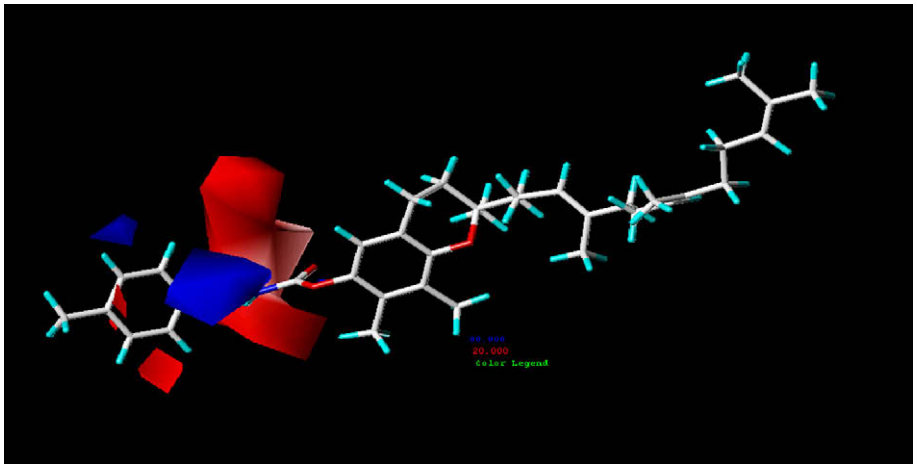

Figure 9. CoMSIA stdev * coeff electrostatic contour plots; blue contours indicate regions where positive groups increase activity, whereas red contours indicate regions where negative charge increases activity.

Table 7
Predicted IC_{50} values of new tocotrienol analogues designed according to multifit-aligned 3D QSAR studies[a]

Compound	Predicted IC_{50}/μM
36	2.03
37	1.82
36	1.30
39	1.70
40	2.31

[a] Predicted activity presents the CoMSIA predictions.

were added. Each solution was separately stirred and refluxed for 3 h. Water (10 mL) then added and each reaction mixture was extracted with EtOAc (3 × 10 mL). Each EtOAc extract was dried over anhydrous Na_2SO_4 and concentrated under vacuum to produce after further column chromatography compounds **4–22**.

(B) Etherification of **1**–**3**.[27] Solutions of **1**–**3** (0.15 mmol) in dry THF were added drop-wise to a cooled (5 °C) oil-free suspension of NaH (0.16 mmol) in 5 mL dry THF. Different alkyl or aryl bromides or chlorides (0.16 mmol) were added drop-wise to the mixture. After hydrogen evolution ceased, the solution was warmed to 23 °C and stirred for 2 h. Each solution was then poured into 1 N NaOH and the mixture was extracted with $CHCl_3$ (3 × 10 mL). Each organic layer was then washed with brine (1 × 10 mL) and dried over anhydrous Na_2SO_4. Crude mixtures were then purified on Si Gel 60 using isocratic $CHCl_3$–methanol (9.9:0.1) system. Evaporation of fractions containing target compounds afforded **23–32** in 70–80% yields.

4.2.1. (*R*)-2,5,7,8-Tetramethyl-2-((3′*E*,7′*E*)-4′,8′,12′-trimethyltrideca-3′,7′,11′-trienyl)chroman-6-yl phenylsulfonylcarbamate (4)

A reaction of 20 mg of **1** with 6.30 μL of benzenesulfonyl isocyanate was carried out give **4**, 40% yield: yellow oil, $[\alpha]_D^{25}$ +18.6 (*c* 0.07, $CHCl_3$); IR ν_{max} ($CHCl_3$) 2929, 1758, 1450, 1405, 1156, 1088, 909 cm^{-1}; ^1H and ^{13}C NMR, see Tables 1 and 2; HRESIMS *m*/*z* 630.3218 $[M+Na]^+$ (calcd for $C_{36}H_{49}NO_5SNa$, 630.3229).

4.2.2. (*R*)-2,7,8-Trimethyl-2-((3′*E*,7′*E*)-4′,8′,12′-trimethyltrideca-3′,7′,11′-trienyl)chroman-6-yl phenylsulfonylcarbamate (5)

Reaction of 100 mg of **2** with 32.63 μL of benzenesulfonyl isocyanate was proceeded to give **5**, 40% yields: yellow oil, $[\alpha]_D^{25}$ +16 (*c* 0.1, $CHCl_3$); IR ν_{max} ($CHCl_3$) 2928, 1765, 1602, 1450, 1409, 1358 cm^{-1}; ^1H and ^{13}C NMR, see Tables S1 and S2; HRESIMS *m*/*z* 616.3068 $[M+Na]^+$ (calcd for $C_{35}H_{47}NO_5SNa$, 616.3073).

4.2.3. (*R*)-2,8-Dimethyl-2-((3′*E*,7′*E*)-4′,8′,12′-trimethyltrideca-3′,7′,11′-trienyl)-chroman-6-yl phenylsulfonylcarbamate (6)

A reaction of 50 mg of **3** with 11.70 μL benzenesulfonyl isocyanate was carried out to give **6**, 40% yield: yellow oil, $[\alpha]_D^{25}$ +30 (*c* 0.1, $CHCl_3$); IR ν_{max} ($CHCl_3$) 2927, 1760, 1450, 1355, 1159, 1089, 880 cm^{-1}; ^1H and ^{13}C NMR, see Tables S1 and S2; HRESIMS *m*/*z* 602.2917 $[M+Na]^+$(calcd for $C_{34}H_{45}NO_5SNa$, 602.2916).

4.2.4. (*R*)-2,5,7,8-Tetramethyl-2-((3′*E*,7′*E*)-4′,8′,12′-trimethyltrideca-3′,7′,11′-trienyl)chroman-6-yl tosylcarbamate (7)

A reaction of 50 mg of **1** with 17.98 μL *p*-toluenesulfonyl isocyanate was carried out give **7**, 50% yield: yellow oil, $[\alpha]_D^{25}$ +28 (*c* 0.35, $CHCl_3$); IR ν_{max} ($CHCl_3$) 2928, 1757, 1355, 1152, 1088, 890 cm^{-1}; ^1H and ^{13}C NMR, see Tables S1 and S2; HRESIMS *m*/*z* 644.3369 $[M+Na]^+$(calcd for $C_{37}H_{51}NO_5SNa$, 644.3386).

4.2.5. (*R*)-2,7,8-Trimethyl-2-((3′*E*,7′*E*)-4′,8′,12′-trimethyltrideca-3′,7′,11′-trienyl)-chroman-6-yl tosylcarbamate (8)

A reaction of 100 mg of **2** with 37.2 μL *p*-toluenesulfonyl isocyanate was carried out to get **8**, 60% yield: yellow oil, $[\alpha]_D^{25}$ −71.6 (*c* 0.06, $CHCl_3$); IR ν_{max} ($CHCl_3$) 2935, 1758, 1458, 1407, 1512, 1152, 1088 cm^{-1}; ^1H and ^{13}C NMR, see Tables 1 and 2; HRESIMS *m*/*z* 630.3244 $[M+Na]^+$ (calcd for $C_{36}H_{49}NO_5SNa$, 630.3229).

4.2.6. (*R*)-2,8-Dimethyl-2-((3′*E*,7′*E*)-4′,8′,12′-trimethyltrideca-3′,7′,11′-trienyl)-chroman-6-yl tosylcarbamate (9)

A reaction of 100 mg of **3** with 38.5 μL *p*-toluenesulfonyl isocyanate was carried out to get **9**, 55% yield: yellow oil, $[\alpha]_D^{25}$ −15.0 (*c* 0.7, $CHCl_3$); IR ν_{max} ($CHCl_3$) 2930, 1753, 1350, 1158, 1089, 909 cm^{-1}; ^1H and ^{13}C NMR, see Tables 1 and 2; HRESIMS *m*/*z* 616.3070 $[M+Na]^+$ (calcd for $C_{35}H_{47}NO_5SNa$, 616.3073).

4.2.7. (*R*)-2,5,7,8-Tetramethyl-2-((3′*E*,7′*E*)-4′,8′,12′-trimethyltrideca-3′,7′,11′-trienyl)-chroman-6-yl-4″ chlorophenylsulfonylcarbamate (10)

A reaction of 100 mg of **1** with 35.17 μL 4-chlorobenzenesulfonyl isocyanate was carried out to get **10** in a 45% yield: yellow oil, $[\alpha]_D^{25}$ −8.3 (*c* 0.6, $CHCl_3$); IR ν_{max} ($CHCl_3$) 2928, 2360, 1757, 1458, 1154, 988 cm^{-1}; ^1H and ^{13}C NMR(Tables 1 and 2); HRESIMS *m*/*z* 664.2840 $[M+Na]^+$ (calcd for $C_{36}H_{48}ClNO_5SNa$, 664.2835).

4.2.8. (*R*)-2,7,8-Trimethyl-2-((3′*E*,7′*E*)-4′,8′,12′-trimethyltrideca-3′,7′,11′-trienyl)-chroman-6-yl-4″-chlorophenylsulfonylcarbamate (11)

A reaction of 100 mg of **2** with 36.4 μL 4-chlorobenzenesulfonyl isocyanate was carried out to get **11**, 40% yield: yellow oil, $[\alpha]_D^{25}$ +5 (*c* 1, $CHCl_3$); IR ν_{max} ($CHCl_3$) 2931, 2360, 1761, 1154, 1091, 893 cm^{-1}; ^1H and ^{13}C NMR, see Tables S3 and S4; HRESIMS *m*/*z* 650.2668 $[M+Na]^+$ (calcd for $C_{35}H_{46}ClNO_5SNa$, 650.2683).

4.2.9. (*R*)-2,8-Dimethyl-2-((3′*E*,7′*E*)-4′,8′,12′-trimethyltrideca-3′,7′,11′-trienyl)-chroman-6-yl-4″-chlorophenylsulfonylcarbamate (12)

A reaction of 100 mg of **3** with 37.60 μL 4-chlorobenzenesulfonyl isocyanate was carried out to get **12** in a 50% yield: yellow oil, $[\alpha]_D^{25}$ −9.0 (*c* 0.1, $CHCl_3$); IR ν_{max} ($CHCl_3$) 2929, 2360, 1758, 1602, 1457, 1360, 978 cm^{-1}; ^1H and ^{13}C NMR, see Tables S3 and S4; HRESIMS *m*/*z* 636.2529 $[M+Na]^+$ (calcd for $C_{34}H_{44}ClNO_5SNa$, 636.2526).

4.2.10. (*R*)-2,5,7,8-Tetramethyl-2-((3′*E*,7′*E*)-4′,8′,12′-trimethyl trideca-3′,7′,11′-trienyl)chroman-6-yl phenylcarbamate (13)

A reaction of 20 mg of **1** with 4.52 μL phenylisocyanate was carried out to get **13** in a 50% yield: yellow oil, $[\alpha]_D^{25}$ +11 (*c* 0.2, $CHCl_3$); IR ν_{max} ($CHCl_3$) 2929, 1731, 1602, 1454, 1104, cm^{-1}; ^1H and ^{13}C NMR, see Tables S3 and S4; HRESIMS *m*/*z* 566.3610 $[M+Na]^+$ (calcd for $C_{36}H_{49}NO_3Na$, 566.3610).

4.2.11. (*R*)-2,7,8-Trimethyl-2-((3′*E*,7′*E*)-4′,8′,12′-trimethyltrideca-3′,7′,11′-trienyl)-chroman-6-yl phenylcarbamate (14)

A reaction of 40 mg of **2** with 12.00 μL phenylisocyanate was carried out to get **14**, 50% yield: yellow oil, $[\alpha]_D^{25}$ +55 (*c* 0.1, $CHCl_3$); IR ν_{max} ($CHCl_3$) 3019, 2400, 1522, 1424, 929 cm^{-1}; ^1H and ^{13}C NMR, see Tables S3 and S4; HRESIMS *m*/*z* 552.3521$[M+Na]^+$ (calcd for $C_{35}H_{47}NO_3Na$, 552.3520).

4.2.12. (*R*)-2,8-Dimethyl-2-((3′*E*,7′*E*)-4′,8′,12′-trimethyltrideca-3′,7′,11′-trienyl)-chroman-6-yl phenylcarbamate (15)

A reaction of 100 mg of **3** with 27.40 μL phenylisocyanate to get **15**, 50% yield: yellow oil, $[\alpha]_D^{25}$ +1.8 (*c* 3.6, $CHCl_3$); IR ν_{max} ($CHCl_3$) 2929, 2854, 1744, 1604, 1442, 1139, 1021 cm^{-1}; ^1H and ^{13}C NMR, see Tables S5 and S6; HRESIMS *m*/*z* 538.3271$[M+Na]^+$ (calcd for $C_{34}H_{45}NO_3Na$, 538.3297).

4.2.13. 13(*R*)-2,5,7,8-Tetramethyl-2-((3′*E*,7′*E*)-4′,8′,12′-trimethy ltrideca-3′,7′,11′-trienyl)-chroman-6-yl benzylcarbamate (16)

A reaction of 40 mg of **1** with 11.63 μL benzylisocyanate was carried out to get **16**, 40% yield: yellow oil, $[\alpha]_D^{25}$ +43 (*c* 0.09, $CHCl_3$); IR ν_{max} ($CHCl_3$) 2927, 1745, 1603, 1443, 1097, cm^{-1}; ^1H and ^{13}C NMR, see Tables 1 and 2; HRESIMS *m*/*z* 580.3766 $[M+Na]^+$ (calcd for $C_{37}H_{51}NO_3Na$, 580.3767).

4.2.14. (*R*)-2,7,8-Trimethyl-2-((3′*E*,7′*E*)-4′,8′,12′-trimethyltrideca-3′,7′,11′-trienyl)-chroman-6-yl benzylcarbamate (17)

A reaction of 50 mg of **2** with16.31 μL benzylsulfonyl isocyanate was carried out to get **17**, 40% yield: yellow oil, $[\alpha]_D^{25}$ +6.0 (*c* 0.1, $CHCl_3$); IR ν_{max} ($CHCl_3$) 2929, 1744, 1603, 1443, cm^{-1}; ^1H and ^{13}C NMR, see Table S5 and S6; HRESIMS *m*/*z* 566.3610 $[M+Na]^+$ (calcd for $C_{36}H_{49}NO_3Na$, 566.3610).

4.2.15. (*R*)-2,8-Dimethyl-2-((3′*E*,7′*E*) 4′,8′,12′-trimethyltrideca-3′,7′,11′-trienyl)chroman-6-yl benzylcarbamate (18)

A reaction of 100 mg of **3** with 31.0 μL benzylsulfonyl isocyanate was carried out to get **18**, 40% yield: yellow oil, $[\alpha]_D^{25}$ +3.0 (*c* 3.55, $CHCl_3$); IR ν_{max} ($CHCl_3$) 2930, 1733, 1471, 1154, 911 cm^{-1}; ^1H and ^{13}C NMR, see Tables S5 and S6; HRESIMS *m*/*z* 552.3444 $[M+Na]^+$ (calcd for $C_{35}H_{47}NO_3Na$, 552.3454).

4.2.16. (*R*)-2,5,7,8-Tetramethyl-2-((3′*E*,7′*E*)-4′,8′,12′-trimethyltrideca-3′,7′,11′-trienyl)chroman-6-yl benzoylcarbamate (19)

A reaction of 100 mg of **1** with 31.2 μL phenylisocyanatoformate was carried out to get **19**, 60% yield: yellow oil, $[\alpha]_D^{25}$ −4 (*c* 1.6, $CHCl_3$); IR ν_{max} ($CHCl_3$) 1823, 1748, 1478, 1143, 1085, 1005 cm^{-1}; ^1H and ^{13}C NMR, see Tables S5 and S6; HRESIMS *m*/*z* 610.3506 $[M+Na]^+$ (calcd for $C_{37}H_{49}NO_5Na$, 610.3508).

4.2.17. (*R*)-2,7,8-Trimethyl-2-((3′*E*,7′*E*)-4′,8′,12′-trimethyltrideca-3′,7′,11′-trienyl)-chroman-6-yl benzoylcarbamate (20)

A reaction of 50 mg of **2** with 32.2 μL phenylisocyanatoformate was carried out to get **20**, 70% yield. Yellow oil, $[\alpha]_D^{25}$ +3.75 (*c* 0.16, $CHCl_3$); IR ν_{max} ($CHCl_3$) 2935, 1822, 1740, 1487, 1141, 1085 cm^{-1}; ^1H and ^{13}C NMR, see Tables S7 and S8; HRESIMS *m*/*z* 596.3333$[M+Na]^+$ (calcd for $C_{36}H_{47}NO_5Na$, 596.3352).

4.2.18. (*R*)-2,8-Dimethyl-2-((3′*E*,7′*E*)-4′,8′,12′-trimethyltrideca-3′,7′,11′-trienyl)-chroman-6-yl benzoylcarbamate (21)

A reaction of 100 mg of **3** with 33.4 μL phenyl isocyanatoformate was carried out to get **21**, 65% yield: yellow oil, $[\alpha]_D^{25}$ +4 (*c* 0.5, $CHCl_3$); IR ν_{max} ($CHCl_3$) 2930, 1824, 1471, 1132, 1056 cm^{-1}; ^1H and ^{13}C NMR, see Tables S7 and S8; HRESIMS *m*/*z* 582.3193$[M+Na]^+$ (calcd for $C_{35}H_{45}NO_5Na$, 582.319).

4.2.19. (*R*)-2,8-Dimethyl-2-((3′*E*,7′*E*)-4′,8′,12′-trimethyltrideca-3′,7′,11′-trienyl) chroman-6-yl naphthalen-1″-ylcarbamate (22)

A reaction of 100 mg of **3** with 37.8 μL 1-naphthylisocyanate was carried out to get **22**, 70% yield: yellow oil, $[\alpha]_D^{25}$ +2 (*c* 1.9, $CHCl_3$); IR ν_{max} ($CHCl_3$) 2928, 1743, 1472, 1348, 1176, 1140, 1000 cm^{-1}; ^1H and ^{13}C NMR, see Tables S7 and S8; HRESIMS *m*/*z* 588.3460$[M+Na]^+$ (calcd for $C_{38}H_{47}NO_3Na$, 588.3454).

4.2.20. (*R*)-2,7,8-Trimethyl-6-(4″-methylpent-3″-enyloxy)-2-((3′*E*,7′*E*)-4′,8′,12′-trimethyltrideca-3′,7′,11′-trienyl)chroman (24)

About 61.5 mg of **2** in 214 μL 5-bromo-2-methylpent-2-ene gave **24**, 70% yield: yellow oil, $[\alpha]_D^{25}$ −30 (*c* 0.35, $CHCl_3$); IR ν_{max} ($CHCl_3$) 2931, 1452, 1379, 1098, 986 cm^1; ^1H and ^{13}C NMR, see Tables S7 and S8; HREIMS *m*/*z* 492.3955 $[M^+]$ (calcd for $C_{34}H_{52}O_2$, 492.3967).

4.2.21. (*R*)-6-(Isopentyloxy)-2,7,8-trimethyl-2-((3′*E*,7′*E*)-4′,8′,12′-trimethyltrideca-3′,7′,11′-trienyl)chroman (25)

Reaction of 61.5 mg of **2** with 191 μL 1-bromo-3-methylbutane gave **25**, 80% yield: yellow oil, $[\alpha]_D^{25}$ +2.2 (*c* 0.85, $CHCl_3$); IR ν_{max} ($CHCl_3$) 2931, 2870, 1466, 1379, 1098, 983 cm^{-1}; ^1H and ^{13}C NMR, see Tables S7 and S8; HREIMS *m*/*z* 480.3952 $[M^+]$ (calcd for $C_{33}H_{52}O_2$, 480.3967).

4.2.22. (*R*)-2,5,7,8-Tetramethyl-6-((2″*E*,6″*E*)-3″,7″,11″-trimethyldodeca-2″,6″,10″-trienyloxy)-2-((3′*E*,7′*E*)-4′,8′,12′-trimethyltrideca-3′,7′,11′-trienyl)chroman (26)

Reaction of **1** (64 mg) with (2*E*,6*E*)-1-bromo-3,7,11-trimethyldodeca-2,6,10-triene (433 μL) gave **26**, 85% yield: yellow oil, $[\alpha]_D^{25}$ −8 (*c* 0.5, $CHCl_3$); IR ν_{max} ($CHCl_3$) 2930, 2856, 1455, 1378, 1086, 976 cm^{-1}; ^1H and ^{13}C NMR, see Tables S9 and S10; HREIMS *m*/*z* 628.5276 $[M^+]$ (calcd for $C_{44}H_{68}O_2$, 628.5219).

4.2.23. (*R*)-2,7,8-Trimethyl-6-((2″*E*,6″*E*)-3″,7″,11″-trimethyldodeca-2″,6″,10′-trienyloxy)-2-((3′*E*,7′*E*)-4′,8′,12′-trimethyltrideca-3′,7′,11′-trienyl)chroman (27)

Reaction of **2** (61.5 mg) with (2*E*,6*E*)-1-bromo-3,7,11-trimethyldodeca-2,6,10-triene (433 μL) afforded **27**, 80% yield: yellow oil, $[\alpha]_D^{25}$ +1.4 (*c* 1.07, $CHCl_3$); IR ν_{max} ($CHCl_3$) 2931, 2856, 2360, 1453, 1397, 1379, 1097, 986 cm^{-1}; ^1H and ^{13}C NMR, see Tables

S9 and S10; HREIMS *m/z* 614.5076 [M$^+$] (calcd for $C_{43}H_{66}O_2$, 614.5063).

4.2.24. (*R*)-2,8-Dimethyl-6-((2″*E*,6″*E*)-3″,7″,11″-trimethyldodeca-2″,6″,10″-trienyloxy)-2-((3′*E*,7′*E*)-4′,8′,12′-trimethyltrideca-3′,7′,11′-trienyl)chroman (28)

Reaction of **3** (59 mg) with (2*E*,6*E*)-1-bromo-3,7,11-trimethyldodeca-2,6,10-triene (433 μL) afforded **28**, 80% yield: yellow oil, $[\alpha]_D^{25}$ +3.2 (*c* 1.55, $CHCl_3$); IR ν_{max} ($CHCl_3$) 2933, 2859, 2340, 1457, 1397, 1379, 986 cm^{-1}; ^{1}H and ^{13}C NMR, see Tables S9 and S10; HREIMS *m/z* 600.4902 [M$^+$] (calcd for $C_{42}H_{64}O_2$, 600.4906).

4.2.25. (*R*)-6-(4″-Methoxybenzyloxy)-2,5,7,8-tetramethyl-2-((3′*E*,7′*E*)-4′,8′,12′-trimethyltrideca-3′,7′,11′-trienyl)chroman (29)

Reaction of **1** (64 mg) with 1-(bromomethyl)-3-methoxybenzene (462 μL) gave **29**, 70% yield: yellow oil, $[\alpha]_D^{25}$ +38 (*c* 0.26, $CHCl_3$); IR ν_{max} ($CHCl_3$) 2938, 2839, 2359, 1457, 1370, 1091, 987 cm^{-1}; ^{1}H and ^{13}C NMR, see Tables S11 and S12; HREIMS *m/z* 544.3916 [M$^+$] (calcd for $C_{37}H_{52}O_3$, 544.3916).

4.2.26. (*R*)-6-(4″-Methoxybenzyloxy)-2,7,8-trimethyl-2-((3′*E*,7′*E*)-4′,8′,12′-trimethyl-trideca-3′,7′,11′-trienyl)chroman (30)

Reaction of **2** (61.5 mg) with 1-(bromomethyl)-3-methoxybenzene (462 μL) afforded **30**, 75% yield: yellow oil, $[\alpha]_D^{25}$ +2.4 (*c* 1.19, $CHCl_3$); IR ν_{max} ($CHCl_3$) 2930, 2855, 2360, 1717, 1604, 1491, 1457, 1378, 1270, 1099, 909 cm^{-1}; ^{1}H and ^{13}C NMR, see Tables S11 and S12; HRESIMS *m/z* 553.3651 [M+Na]$^+$ (calcd for $C_{36}H_{50}O_3Na$, 553.3658).

4.2.27. (*R*)-6-(4″,6″-Dimethoxybenzyloxy)-2,5,7,8-tetramethyl-2-((3′*E*,7′*E*)-4′,8′,12′-trimethyltrideca-3′,7′,11′-trienyl)chroman (31)

Reaction of **1** (64 mg) with 1-(bromomethyl)-3,5-dimethoxybenzene (37 mg) afforded **31**, 80% yield: yellow oil, $[\alpha]_D^{25}$ −14.8 (*c* 0.27, $CHCl_3$); IR ν_{max} ($CHCl_3$) 2931, 2856, 1599, 1458, 1370, 1155, 1089, 993 cm^{-1}; ^{1}H and ^{13}C NMR, see Tables S11 and S12; HREIMS *m/z* 574.4015 [M+] (calcd for $C_{38}H_{54}O_4$, 574.4022).

4.2.28. (*R*)-6-(4″,6″-Dimethoxybenzyloxy)-2,7,8-trimethyl-2-((3′*E*,7′*E*)-4′,8′,12′-trimethyltrideca-3′,7′,11′-trienyl) chroman (32)

Reaction of **2** (61.5 mg) with 1-(bromomethyl)-3,5-dimethoxybenzene (37 mg) afforded **32**, 85% yield: yellow oil, $[\alpha]_D^{25}$ 1.03 (*c* 1.65, $CHCl_3$); IR ν_{max} ($CHCl_3$) 2939, 2841, 1599, 1461, 1157, 1099, 1068, 993, 838 cm^{-1}; ^{1}H and ^{13}C NMR, see Tables S13; HRESIMS *m/z* 583.3753 [M+Na]$^+$ (calcd for $C_{37}H_{52}O_4Na$, 583.3763).

4.3. Cell culture

Breast cancer cell lines, MCF7 and MDA-MB-231 were purchased from ATCC (Manassas, VA). The cell lines were grown in 10% fetal bovine serum (FBS) and RPMI 1640 (GIBCO-Invitrogen, NY) supplemented with 2 mmol/L glutamine, 100 μg/mL penicillin G, and 100 μg/mL streptomycin, at 37 °C under 5% CO_2.

4.4. Proliferation assay

The antiproliferative effects of tocotrienol analogues were tested in culture on the highly malignant +SA mouse mammary epithelial cell line maintained on serum free media and containing 10 ng/mL EGF and 10 μg/mL insulin as mitogens, as described previously in detail.[28] Cells were plated at a density of 5×10^4 cells/well (6 wells/group) in 24-well culture plates and fed media containing various concentrations (0.01–1000 μM) of each compound. After a four-day culture period, viable +SA cell number was determined by the MTT colorimetric assay as described previously.[23] The cells growth of MCF7 and MDA-MB-231 cell lines was measured using MTT kit (TACS™, Trevigen®, Inc.). After passing the cells for 3–4 times, growing cells were incubated in a 96 well plate at a density of 8×10^3 cells per well, and allowed to attach for 24 h. Complete growth medium was then replaced with 100 μL of RPMI of serum free medium (GIBCO-Invitrogen, NY) containing various doses (20, 10, 5, 2 μM) of the specific compound and culture will continued at 37 °C under 5% CO_2. After 96 h, the incubated cells were treated with MTT solution (10 μL/well) at 37 °C for 4 h. The color reaction stopped by the addition of solubilization/stop solution (100 μL/well), and the incubation at 37 °C continued to completely dissolve the formazan product. Absorbance of the samples was determined at 570 nm with an ELISA plate reader (BioTek, VT). The number of cells per well was calculated against a standard curve prepared by plating various concentration of cells, as determined by hemocytometer, at the start of each experiment. IC_{50} for the compound was calculated using nonlinear regression (curve fit) of log concentration versus number of cells/well implemented in GraphPad Prism 5.0.

Growth curves were determined to ensure that cells used in experiments were within the exponential growth phase. Cell proliferation was assessed by monitoring the conversion of MTT to formazan. The reduction of MTT is catalyzed by mitochondrial dehydrogenase enzymes and is therefore a measure for cell viability. Briefly, cells (100 μL/well) were seeded at seeding densities of 1×10^5, 1×10^4 or 1×10^3 cells/ml into 96 well microtitre plates and allowed to adhere for 24 h. Cell viability was assessed on a daily basis by adding 10 μL of filter sterilized MTT (5 mg/mL in PBS) to a each well. Following a 4 h incubation period with MTT, 100 μL of solubilizing agent was added to each well, and the blue formazan crystals trapped in cells dissolved at 37 °C for 2–4 h or at room temperature for over night in dark place. The absorbance at 550 nm was measured with a plate reader.

4.5. Cell invasion assay

Anti-invasive activities were measured using Trevigen's Cultrex® Cell Invasion Assay.[29,30] About 50 μL of (BME 1X) coat was added per well. After incubation for overnight at 37 °C in a 5% CO_2, 50,000/50 μL of MDA-MB-231 cells in serum free RPMI medium were added per well to top chamber containing the tested compound at treatment concentration (5 μM). About 150 μL of RPMI medium was added to lower chamber containing 10% FBS (chemoattractant) and penicillin/streptomycin and using fibronectin (1 μL/mL) and *N*-formyl-met-leu-phe (10 nM) as chemoattractants. Cells were allowed to migrate to lower chamber at 37 °C in CO_2 incubator. After 24 h, top and bottom chambers were aspirated and washed with wash buffer supplemented with the kit. About 100 μL of cell dissociation/calcein–AM solution was added to the bottom chamber and incubated at 37 °C in CO_2 incubator for 1 h. The cells internalize calcein–AM, and the intracellular esterases cleaved the AM moiety to generate free calcein. Fluorescence of the samples was determined at 485 nm excitation, 520 nm emission using plate reader (BioTek Synergy 2, VT). The numbers of cells that have invaded through the BME coat were calculated using a standard curve.

4.6. Chemicals and reagents

All isocyanates reagents have been purchased from Sigma–Aldrich. (TRF) 50 g (Palm TRF 70%, low in tocopherol from First Tech International Ltd, Hong Kong) was fractionated using Si Gel 60 VLC with *n*-hexane–ethyl acetate (gradient elution) as a mobile phase.

4.7. CoMFA and CoMSIA

Three-dimensional structure building was performed using the SYBYL program package, version 8.1, installed on DELL desktop workstations equipped with a 1.8 GHz Intel® Xeon® processor running the Red Hat Enterprise Linux (version 5.0) operating system. For the calculating of charges, the Gasteiger-Hückel method was used as implemented in SYBYL.[31]

CoMSIA analysis was performed using the QSAR module in SYBYL 8.1. The five similarity indices in CoMSIA (steric (S), electrostatic (E), hydrophobic (H), H-bond donor (D), and H-bond acceptor (A) descriptors) were calculated using the probe atom Csp_3 + with a radius of 1 Å and a +1.0 charge placed at the lattice points of the same region of grid as it was used for the CoMFA calculations. CoMSIA similarity indices (*AF*) for a molecule *j* with atom *i* at a grid point *q* are calculated by the equation:

$A_{F,kq}(j) = -\sum \omega_{\text{probe, k}}\omega_{ik}\, e^{-\alpha r i q^2}$, where *k* represents the following physicochemical properties: steric, electrostatic, hydrophobic, HBD, and HBA. A Gaussian type distance dependence was used between the grid point *q* and each atom *i* of the molecule. A default value of 0.3 was used as the attenuation factor (*R*). Here, steric indices are related to the third power of the atomic radii, electrostatic descriptors are derived from atomic partial charges, hydrophobic fields are derived from atom-based parameters.[32]

4.8. Partial least-squares (PLS) analysis

The statistical method used in deriving the 3D QSAR models, is a variation of principal component regression[33] in which the original variables are replaced by a small set of linear combinations thereof. The latent variables so generated are used for multivariate regression, maximizing the communality of predictor and response variable blocks. PLS has several attractive features, such as: (i) the ability to handle multivariate regression analysis in cases where the number of independent variables is greater than the number of compounds as found in CoMFA and CoMSIA 3D QSAR analyses; (ii) the ability to perform well even when inter-descriptor correlations exist that would pose a problem for traditional multiple linear regression; (iii) the reduction of the risk of chance correlations.[33,34]

Initial the leave-one-out (LOO) cross-validated PLS analyses were used to determine the optimum number of components to be used in the final 3D QSAR models. The leave-one-out cross-validation method might lead to high q^2 values, which do not necessarily reflect a general predictiveness of the models. Therefore, we have performed cross-validation using two groups (leave-half-out) in CoMFA study. In this method 50% of the compounds were randomly selected and a model was generated, which was then used to predict the activity of the remaining 50% of compounds. The random formation of the cross-validation groups may have an effect on the results; hence cross-validation was performed 100 times for all the analysis.[33,34]

The conventional CoMFA and CoMSIA descriptors derived above were used as explanatory variables, and pIC_{50} ($-\log IC_{50}$) values (Tables 4 and 5) were used as the target variable in PLS regression analyses to derive 3D QSAR models using the implementation in the SYBYL package. The predictive value of the models was evaluated by LOO cross validation with SAMPLS. The cross-validated coefficient, q^2, was calculated using the equation:$q^2 = 1 - \sum(Y_{\text{pred}} - Y_{\text{actual}})^2/\sum(Y_{\text{actual}} - Y_{\text{mean}})^2$, where Y_{pred}, Y_{actual}, and Y_{mean} are predicted, actual, and mean values of the target property (pIC_{50}), respectively. $\sum(Y_{\text{pred}} - Y_{\text{actual}})^2$ is the predictive sum of squares (PRESS). The number of components giving the lowest PRESS value or the optimal number of components (ONC) was used to generate the final PLS regression models. The conventional correlation coefficient r^2 and its standard error, *s*, were subsequently computed for the final PLS models.

In order to have sufficient number of compounds with activity variation for PLS analysis, the previously published tocopherol analogues **33**–**35** have been added to a database set of 29 tocotrienol derivatives.[35,36] This dataset of total number 32 tocotrienol and tocopherol analogues were used for both CoMFA and CoMSIA studies based on the antiproliferative effect against MCF-7 breast cancer cell line using MTT-assay. The pIC_{50} ($-\log IC_{50}$), which is responsible for 50% inhibition of cells growth, was used in these studies. The 32 compounds were divided to training set comprising 27 compounds (Table 5), 84% of database set, and test set, five compounds, 16% of the set (Table 4).

For deriving the CoMFA and CoMSIA descriptor fields, the molecules from the training set were placed in a three dimensional cubic lattice with a spacing of 2 Å and extending 4 Å units beyond the aligned molecules in all directions. CoMFA descriptors were calculated using an sp3 carbon probe atom with a van der Waals radius of 1.52 Å and a charge of +1.0 with a distance-dependent dielectric to generate steric (Lennard-Jones 6–12 potential) field energies and electrostatic (Columbic potential) fields with a distance-

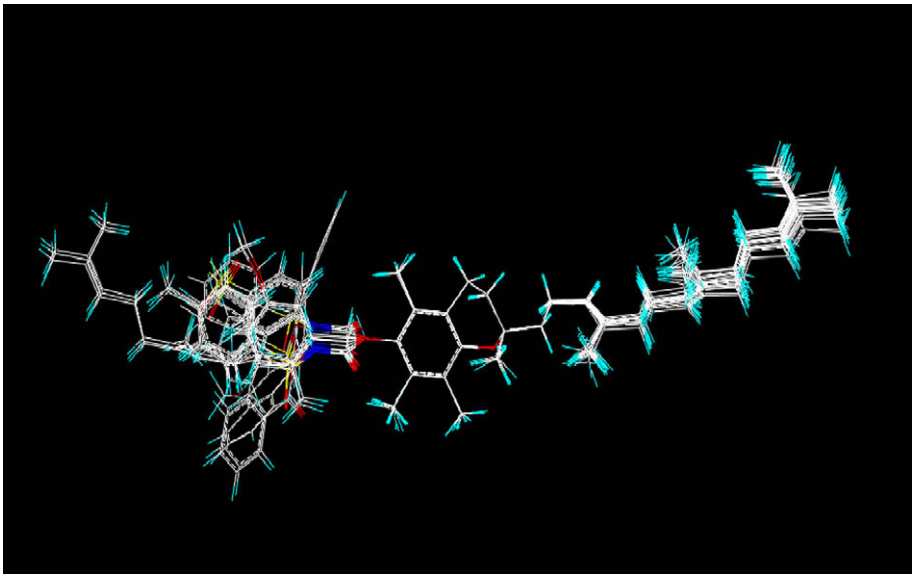

Figure 10. Superposition of tocotrienols training and test sets using field fit alignment.

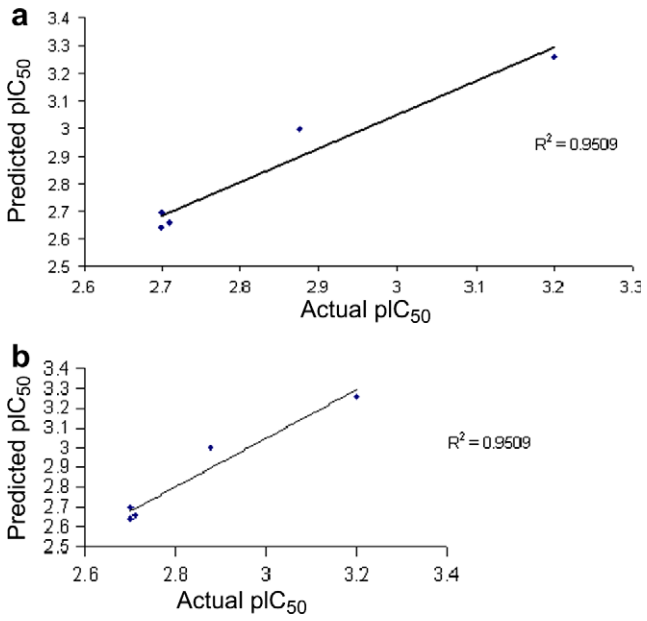

Figure 11. Prediction curves for CoMFA (a) and CoMSIA (b) model-predicted pIC_{50} for the test set of MCF-7 proliferation inhibition.

dependent dielectric at each lattice point. An energy cutoff of 30 kcal/mol was applied. The CoMFA steric and electrostatic fields were scaled by the CoMFA-STD method in SYBYL.[37] Tables 4 and 5 show the actual and predicted activity for both test and training sets respectively. The predicted activities of training and test set values were obtained by multiplying the values of each descriptors for a particular row generated by CoMFA, CoMSIA by their corresponding coefficient from the PLS equation in the model and this can be translated through prediction curves for CoMFA and CoMSIA model-predicted pIC_{50} for the test set of MCF-7 proliferation inhibition as shown in Figure 11.

4.9. Alignment rule

The alignment rule is one of the most sensitive input areas for CoMFA studies. The SYBYL QSAR rigid body field fit command was used for this alignment. Field uses a simplex algorithm in SYBYL that minimizes the differences in steric and electrostatic fields averaged over all the lattice grid points to find the best fit. The most active tocotrienol **8** was used as a reference and there is also a skeleton structure, without hydrogen atoms, was used as common compound on which other molecules were aligned as showed in Figure 10. Values of the steric and electrostatic fields were truncated at 30 kcal/mol.

Acknowledgment

This work was supported in part by a grant from First Tech International Ltd.

Supplementary data

Supplementary data associated with this article can be found, in the online version, at doi:10.1016/j.bmc.2009.11.054.

References and notes

1. Sen, C. K.; Khanna, S.; Roy, S.; Packer, L. *J. Biol Chem.* **2000**, *275*, 13049.
2. Crowell, P. L.; Chang, R. R.; Ren, Z. B.; Elson, C. E.; Gould, M. N. *J. Biol. Chem.* **1991**, *266*, 17679.
3. Elson, C. E.; Yu, S. G. *J. Nutr.* **1994**, *124*, 607.
4. McIntyre, B.; Briski, K. P.; Gapor, A.; Sylvester, P. W. *Proc. Soc. Exp. Biol. Med.* **2000**, *224*, 292.
5. Sporn, M. B.; Suh, N. *Nat. Rev. Cancer* **2002**, *2*, 537.
6. Shukla, S.; Gupta, S. *Nutr. Cancer* **2005**, *53*, 18.
7. Nesaretnam, K.; Guthrie, N.; Chambers, A. F.; Carroll, K. K. *Lipids* **1995**, *30*, 1139.
8. Qureshi, A. A.; Sami, S. A.; Salser, W. A.; Khan, F. A. *Atherosclerosis* **2002**, *161*, 199.
9. Khanna, S.; Roy, S.; Ryu, H.; Bahadduri, P.; Swaan, P. W.; Ratan, R. R. *J. Biol. Chem.* **2003**, *278*, 43508.
10. Akaho, N.; Takata, J.; Fukushima, T.; Matsunaga, K.; Hattori, A.; Hidaka, R.; Fukui, K.; Yoshida, M.; Fujioka, T. R.; Karube, Y.; Imai, K. *Drug Metab. Dispos.* **2007**, *35*, 1502.
11. Takata, J.; Hidaka, R.; Yamasaki, A.; Hattori, A.; Fukushima, T.; Tanabe, M.; Matsunaga, K.; Karube, Y.; Imai, K. *J. Lipid Res* **2002**, *43*, 2196.
12. Mazzini, F.; Netscher, T.; Salvadori, P. *Eur. J. Org. Chem.* **2009**, *13*, 2063.
13. Tomic-Vatic, A.; EyTina, J.; Chapman, J.; Mahdavian, E.; Neuzil, J.; Salvatore, B. *Int. J. Cancer* **2005**, *117*, 188.
14. Kashiwagi, K.; Harada, K.; Yano, Y.; Kumadaki, I.; Hagiwara, K.; Takebayashi, J.; Kido, W.; Virgona, N.; Yano, T. *Biochem. Biophys. Res. Commun.* **2008**, *365*, 875.
15. Ali, H.; Nazzal, S. *J. Pharm. Biomed. Anal.* **2009**, *49*, 950.
16. Ohnmacht, S.; West, R.; Simionescu, R.; Atkinson, J. *Magn. Reson. Chem.* **2008**, *46*, 287.
17. Shah, S. J.; Sylvester, P. W. *Exp. Biol. Med.* **2005**, *230*, 235.
18. Liu, H.-K.; Wang, Q.; Li, Y.; Sun, W.-G.; Liu, J.-R.; Yang, Y.-M.; Xu, W.-L.; Sun, X.-R.; Chen, B.-Q., *J. Nutr. Biochem*., in press. doi:10.1016/j.jnutbio.2008.11.004).
19. Chang, P.; Yap, W.; Lee, W. D.; Ling, M. T.; Wong, Y. C.; Yap, Y. *Nutr. Cancer* **2009**, *61*, 357.
20. Yap, W. N.; Chang, P. N.; Han, H. Y.; Lee, D. T. W.; Ling, M. T.; Wong, Y. C.; Yap, Y. L. *Br. J. Cancer* **2008**, *99*, 1832.
21. Tamilarasan, K. P.; Kolluru, G. K.; Rajaram, M.; Indhumathy, M.; Saranya, R.; Chatterjee, S. B. M. C. *Cell Biol.* **2006**, *7*, 17.
22. Borghesani, P. R.; Peyrin, J. M.; Klein, R.; Rubin, J.; Carter, A. R.; Schwartz, P. M.; Luster, A.; Corfas, G.; Segal, R. A. *Development* **2002**, *6*, 1435.
23. Kubinyi, H., 5th ed.. In *Burger's Medicinal Chemistry*; Wolff, M. E., Ed.; Wiley: New York, 1995; Vol. I, pp 497–571.
24. Arya, P.; Alibhai, N.; Qin, H.; Batist, G.; You, S.; Alaoui-Jamali, M. *Bioorg. Med. Chem. Lett.* **1998**, *8*, 2433.
25. Pearlman, R. S. *3D QSAR in Drug Design. Theory, Methods, and Applications*; ESCOM Science: Leiden, The Netherlands, 1993.
26. El Sayed, K.; Khanfar, M.; Shallal, H.; Muralidharan, A.; Awate, B.; Youssef, D.; Shah, G. *J. Nat. Prod.* **2008**, *71*, 396.
27. Pearce, B.; Parker, R.; Deason, M.; Qureshi, A.; Wright, K. *J. Med. Chem.* **1992**, *35*, 3595.
28. Denizot, F.; Lang, R. *J. Immunol. Methods* **1986**, *89*, 271.
29. Kleinman, H. K.; Martin, G. R. *Semin. Cancer Biol.* **2005**, *15*, 378.
30. Koblinski, J. E.; Kaplan-Singer, B. R.; van Osdol, S. J.; Wu, M.; Engbring, J. A.; Wang, S.; Goldsmith, C. M.; Piper, J. T.; Vostal, J. G.; Harms, J. F.; Welch, D. R.; Kleinman, H. K. *Cancer Res.* **2005**, *65*, 7370.
31. Gupte, A.; Buolamwini, J. *Bioorg. Med. Chem. Lett.* **2009**, *19*, 314.
32. Viswanadhan, V. N.; Ghose, A. K.; Revankar, G. R.; Robins, R. K. *J. Chem. Inf. Comput. Sci.* **1989**, *29*, 163.
33. Wold, S.; Rhue, A.; Wold, H.; Dunn, W. J. *SAIM J. Sci. Stat. Comput.* **1994**, *5*, 735.
34. Wold, S.; Albano, C.; Dunn, W. J., III; Edlund, U.; Esbensen, K.; Geladi, P.; Hellberg, S.; Johanson, E.; Lindberg, W.; Sjostrom, M. *NATO Sci. Ser., Ser. C* **1984**, *138 (Chemometrics)*, 17.
35. Nikolic, K.; Agababa, D. *J. Mol. Graph. Model.* **2009**, *27*, 777.
36. Nikolic, K. *J. Mol. Graph. Model* **2008**, *26*, 868.
37. Matter, H.; Will, D.; Nazare, M.; Schreuder, H.; Laux, V.; Wehner, V. *J. Med. Chem.* **2005**, *48*, 3290.